# RIS-Aided Near-Field MIMO Communications: Codebook and Beam Training Design

Suyu Lv<sup>10</sup>, Graduate Student Member, IEEE, Yuanwei Liu<sup>10</sup>, Fellow, IEEE, Xiaodong Xu<sup>10</sup>, Senior Member, IEEE, Arumugam Nallanathan<sup>10</sup>, Fellow, IEEE, and A. Lee Swindlehurst<sup>10</sup>, Fellow, IEEE

Abstract—Downlink reconfigurable intelligent surface (RIS)assisted multi-input-multi-output (MIMO) systems are considered with far-field, near-field, and hybrid-far-near-field channels. According to the angular or distance information contained in the received signals, 1) a distance-based codebook is designed for near-field MIMO channels, based on which a hierarchical beam training scheme is proposed to reduce the training overhead; 2) a combined angular-distance codebook is designed for hybrid-far-near-field MIMO channels, based on which a two-stage beam training scheme is proposed to achieve alignment in the angular and distance domains separately. For maximizing the achievable rate while reducing the complexity, an alternating optimization algorithm is proposed to carry out the joint optimization iteratively. Specifically, the RIS coefficient matrix is optimized through the beam training process, the optimal combining matrix is obtained from the closedform solution for the mean square error (MSE) minimization problem, and the active beamforming matrix is optimized by exploiting the relationship between the achievable rate and MSE. Numerical results reveal that: 1) the proposed beam training schemes achieve near-optimal performance with a significantly decreased training overhead; 2) compared to the angular-only far-field channel model, taking the additional distance information into consideration will effectively improve

Manuscript received 13 August 2023; revised 10 January 2024 and 15 April 2024; accepted 16 April 2024. Date of publication 1 May 2024; date of current version 12 September 2024. This work was supported in part by the National Key Research and Development Program of China under Grant 2020YFB1806905, in part by the National Natural Science Foundation of China under Grant 62201079, in part by China Scholarship Council, in part by the Major Key Project of Peng Cheng Laboratory (PCL), and in part by U.S. National Science Foundation under Grant CCF-2225575 and Grant CNS-2107182. The associate editor coordinating the review of this article and approving it for publication was H. Q. Ngo. (Corresponding author: Xiaodong Xu.)

Suyu Lv is with the State Key Laboratory of Networking and Switching Technology, Beijing University of Posts and Telecommunications, Beijing 100876, China (e-mail: lvsuyu@bupt.edu.cn).

Yuanwei Liu and Arumugam Nallanathan are with the School of Electronic Engineering and Computer Science, Queen Mary University of London, E1 4NS London, U.K. (e-mail: yuanwei.liu@qmul.ac.uk; a.nallanathan@qmul.ac.uk).

Xiaodong Xu is with the State Key Laboratory of Networking and Switching Technology, Beijing University of Posts and Telecommunications, Beijing 100876, China, and also with the Department of Broadband Communication, Peng Cheng Laboratory, Shenzhen, Guangdong 518066, China (e-mail: xuxiaodong@bupt.edu.cn).

A. Lee Swindlehurst is with the Center for Pervasive Communications and Computing, Henry Samueli School of Engineering, University of California at Irvine, Irvine, CA 92697 USA (e-mail: swindle@uci.edu).

Color versions of one or more figures in this article are available at https://doi.org/10.1109/TWC.2024.3393412.

Digital Object Identifier 10.1109/TWC.2024.3393412

the achievable rate when carrying out beam design for near-field communications.

Index Terms—Beam training, codebook, multi-input-multi-output (MIMO), near-field communications (NFC), reconfigurable intelligent surface (RIS).

#### I. INTRODUCTION

ILLIMETER wave (mmWave) communications (30 - 300 GHz) and Terahertz (THz) communications (0.1 - 10 THz) have been recognized as promising candidate technologies for future B5G/6G networks to realize the communication goals of ultra-wide bandwidth and ultra-high transmission rate [1], [2], [3]. Although possessing extremely high bandwidth, mmWave and THz communication suffer from high propagation losses due to penetration, reflection and diffraction, resulting in a reduced link budget compared to that in the sub-6 GHz scenario [4].

To tackle the problems caused by high-frequency communications, reconfigurable intelligent surface (RIS) technology has received extensive research attention due to its distinctive capability of restructuring the wireless propagation environment and establishing additional reliable reflection-based links between the base station (BS) and the user [5], [6]. RISs consist of numerous passive controllable reflecting elements that can adjust the phase shift of incident signals with extremely low power consumption, and thus have been regarded as one of the main enabling solutions to achieve green communication and coverage extension for next-generation wireless systems [7].

The low-cost and low-complexity characteristics of RIS reflecting elements have also promoted the emergence of extremely large-scale RIS to realize higher array gain. However, with an increase in the number of RIS reflecting elements, the boundary separating the near-field communication (NFC) region and far-field communication (FFC) region becomes more distant from the RIS, making the near-field region non-negligible [8], [9], [10]. In contrast to the *plane wave* model in the far-field region, the electromagnetic structure in the near-field region is fundamentally different and the *spherical wave* model should be used [8]. The spherical-wave propagation model for NFC contains both angular and distance information, which allows the resulting beam patterns to focus on a specific point [9]. Thus, NFC can utilize the new dimension of distance

1536-1276 © 2024 IEEE. Personal use is permitted, but republication/redistribution requires IEEE permission. See https://www.ieee.org/publications/rights/index.html for more information.

to realize more precise signal enhancement, interference management and user localization for RIS-assisted wireless networks [11], [12], [13], [14].

However, reliable phase shift design for RIS-assisted communication systems relies heavily on accurate channel state information (CSI), which is challenging to obtain due to the passive property of RISs. In addition, the massive number of RIS elements in a multi-input-multi-output (MIMO) system will also lead to extremely large pilot overhead and high channel estimation complexity. The authors in [15] proposed a two-stage channel estimation procedure in XL-RIS-aided mmWave system to decrease pilot use and computational complexity, where the angular-domain parameters and cascaded angular-polar-domain parameters are estimated separately. A hybrid-field XL-RIS-aided channel model was considered in [16], where the unknown visual region issues caused by the random blockages were taken into consideration. A near-field channel estimation and localization algorithm was proposed in [17] for XL-RIS THz system, leveraging the second-order Fresnel approximation derived from the near-field channel model. Compared to cascaded channel estimation based on least squares or minimum mean squared error, codebookbased beam training has been widely adopted for mmWave or THz communication systems [18], [19], [20]. The beam training method can obtain CSI by estimating the physical directions of channel paths rather than the entire channel, thus realizing lower complexity. Moreover, beam training can directly achieve reliable beamforming by selecting a phaseshift vector from among a set of pre-defined "codewords" during the training procedure, and thus is considered to be an efficient approach to acquire CSI in RIS-assisted wireless communication systems [21], [22], [23]. Existing codebook design and beam training schemes cannot be directly applied to RIS-assisted NFC systems or hybrid FFC & NFC systems.

Codebooks designed for FFC are mainly based on angular information, which is reasonable because the distance from any point on the transmitter to any point on the receiver can be considered equal, and the phase of electromagnetic waves received by different antennas is a linear function of the antenna index in FFC. However, in NFC, the phase of the electromagnetic waves received by different antennas is no longer a linear function of the antenna index, but is related to the distance between specific two points at the receiving and transmitting ends. In addition, channel responses can be decomposed into the Kronecker product of two vectors related to angle of arrival (AoA) and angle of departure (AoD) in FFC, which is no longer applicable in NFC due to the coupling between angle and distance, bringing more difficulties to the design of near-field codebooks.

Furthermore, in RIS-assisted communication systems, BS-RIS link and RIS-user link may be in either far-field or near-field situations, so there may be a mixture of far and near fields. In such cases, the degree of difficulty of codebook design will increase because it is necessary to comprehensively consider the channel conditions of the two links, and as a result, the size of the codebook will also become large. Designing an efficient and accurate beam training method is also a challenge.

#### A. Prior Works

- 1) Channel Modeling for NFC: Signals in the far field of an array lead to planar wavefronts that produce linear phase variations and negligible amplitude differences across the array. However, the situation is different for near-field signals. In order to achieve better performance through reasonable resource allocation, accurate channel models are essential for NFC. Hybrid-field channel modeling schemes were studied in [24] and [25], where the far-field and near-field components are separately estimated. A polar-domain representation for near-field channel models was proposed in [26], accounting for the information in both the angular and distance domains. Considering the different multi-path characteristics observed by antennas at different distances in large-scale MIMO NFC systems, the authors in [27] proposed a non-stationary distance modeling framework.
- 2) Beam Training Schemes: The beam training process is implemented by searching for the optimal beam from multiple predefined directional beams (codewords). For beam training, testing all codewords in the codebook during the training process is the most straightforward approach. However, the codebook and the resulting training overhead can be extremely large for large-scale massive MIMO systems, especially when considering both angular and distance information in NFC. The authors in [18] proposed a new hierarchical codebook to achieve uniform beam alignment performance with low overhead for mmWave communication systems. For mmWave and sub-THz systems with multiple users, [4] and [19] proposed hierarchical beamforming training strategies to carry out simultaneous training for multiple users. Aiming at overcoming the resolution limit of directional angle estimation, [28] proposed a codebook-based beam search approach for mmWave massive MIMO transmissions. However, these codebooks are designed for the far-field case. Considering the spherical wavefront propagation model for NFC, [20], [29] proposed two-phase beam training methods to sequentially perform the beam sweeping in the angular and distance domains. The authors in [30] proposed a novel spatial-chirp codebook and subsequently proposed a slope-domain-based hierarchical update policy, where the upper-layer beam searching range was uniformly divided into several sub-ranges.
- 3) Beam Training Design for RISs: To implement beam training for RIS-based systems, one must first construct an appropriate RIS codebook based on information about the cascaded channel. Then, based on the information obtained during the training phase, the RIS selects the optimal codeword from the predesigned codebook to perform passive beamforming. For RISs with massive numbers of elements, highly efficient beam training schemes with good performance are required to reduce the training overhead. The authors in [22] first proposed a hierarchical codebook-generating method using pattern synthesis, then provided a hierarchical beam training method using two multi-mainlobe codewords in each layer. To train multiple users at the same time, a multi-lobe beam training mechanism was proposed in [31] based on the BS-RIS joint codebook, thus achieving reduced overhead.

A multi-beam training method was proposed for a RIS-assisted multiuser system in [32], by dividing the RIS into multiple sub-surfaces and designing multi-beam directions over time. Although [23], [33], [34] proposed beam training schemes for RIS-assisted NFC systems, only limited scenarios with single-antenna users were considered.

#### B. Motivation and Contributions

As the size of the RIS increases, the near-field region becomes non-negligible. In NFC, CSI is not only related to the angle but also distance, thus the acquisition of CSI becomes very important for proper beam design. The methods for obtaining CSI can be roughly classified into two categories: channel estimation and beam training [34]. In this article, we consider the use of beam training to simultaneously estimate the channel parameters and perform passive beamforming [35], which is simpler than performing channel estimation first and then separately determining the optimal beamforming.

Although there are numerous beam training schemes for FFC, codebook and beam training design for NFC are still in their infancy, especially for RIS-assisted systems. Moreover, the effect of different channel modeling methods for FFC and NFC has not been well investigated. In order to fill this gap, in this article we focus on four different channel models for downlink MIMO RIS-aided systems. Furthermore, we design codebooks and beam training schemes for near-field and mixed-far-near-field channels, which are further used for RIS reflecting coefficient optimization. The main contributions of our work are listed as follows:

- 1) We consider four different channel models for a downlink RIS-assisted MIMO system, namely, i) FF: far-field model for both BS-RIS and RIS-user links; ii) NF: near-field model for BS-RIS link, far-field model for RIS-user link; iii) FN: far-field model for BS-RIS link, near-field model for RIS-user link; iv) NN: near-field model for both BS-RIS and RIS-user links. Here, the assumption of far-field propagation leads to a *planar-wave* channel model, while near-field propagation leads to a *spherical-wave* channel model.
- 2) According to the angular or distance information contained in the received signals, we design i) a distance-based codebook for the NN channel model, based on which we propose a hierarchical beam training scheme to reduce the training overhead; ii) a combined angular-distance codebook for NF and FN channel models, based on which we propose a two-stage beam training scheme to achieve alignment in the angular and distance domains separately.
- 3) To maximize the achievable rate, we propose an alternating optimization (AO) algorithm to carry out the joint optimization of the RIS coefficients and the transmit and receive beamformers in an iterative manner. Specifically, the RIS coefficient matrix is obtained by the proposed beam training schemes, the optimal combining matrix at the user is obtained from the closed-form solution for the mean square error (MSE) minimization

- problem, and the active beamforming matrix at the BS is optimized by exploiting the relationship between the achievable rate and the MSE.
- 4) We present numerical results revealing that: i) the proposed hierarchical and two-stage beam training approaches yield achievable rate performance similar to the exhaustive search (ES) method while significantly reducing the training overhead; ii) compared to angularonly far-field channel models, the achievable rate is improved by exploiting the additional distance information when performing the beam design for NFC.

The organization for the rest of this article is as follows. In Section II, we describe the proposed RIS-assisted MIMO system and the four considered channel models. In Section III, we design different codebooks for the different channel models based on the angular or distance information in the received signals. In Section IV, we propose an AO algorithm to carry out the joint optimization in an iterative manner for maximizing the achievable rate. In particular, two beam training algorithms are proposed in Section IV-A based on the predesigned codebooks, the combining matrix optimization is given in Section IV-B, and the active beamforming matrix optimization is described in Section IV-C. Simulation results and conclusions are given in Section V and Section VI, respectively.

#### II. SYSTEM MODEL

We consider a RIS-assisted downlink communication scenario, where a single multi-antenna BS serves a multi-antenna user. The direct path between the BS and the user is assumed to be blocked due to the existence of propagation obstacles. The BS is equipped with an  $N_{\rm B}$ -element uniform linear array (ULA) of antennas, and the user is equipped with an  $N_{\rm U}$ -element ULA. The RIS consists of a uniform planar array (UPA) with  $M=M_xM_y$  passive reflecting elements, where  $M_x$  and  $M_y$  denote the number of elements along the horizontal axis and vertical axis, respectively.

Four different channel models are considered for the RIS-assisted communication system, as shown in Fig. 1. Specifically, these four channel models are respectively abbreviated as (a) FF: far-field model for both BS-RIS and RIS-user links; (b) NF: near-field model for BS-RIS link, far-field model for RIS-user link; (c) FN: far-field model for BS-RIS link, near-field model for RIS-user link; (d) NN: near-field model for both BS-RIS and RIS-user links. We assume that the system operates at a frequency of  $f_c$ , so the wavelength of the signal is  $\lambda_c = \frac{c}{f}$ . Denote the array spacing as d, which we will assume here to be  $d=\lambda_c/2$ . Denote the array apertures of the BS, RIS and user as  $D_B$ ,  $D_R$  and  $D_U$ , respectively. For the BS and the user with ULAs, the array apertures are calculated as  $D_{\rm B} = (N_{\rm B} - 1) d$  and  $D_{\rm U} = (N_{\rm U} - 1) d$ , respectively; for the RIS with a UPA, the array aperture is calculated as  $D_{\rm R} = \sqrt{[(M_x - 1) d]^2 + [(M_y - 1) d]^2}$ . The comparison between the far-field region and near-field region in RISassisted systems is summarized in TABLE I, including the Rayleigh boundary when  $d = \lambda_c/2$ .

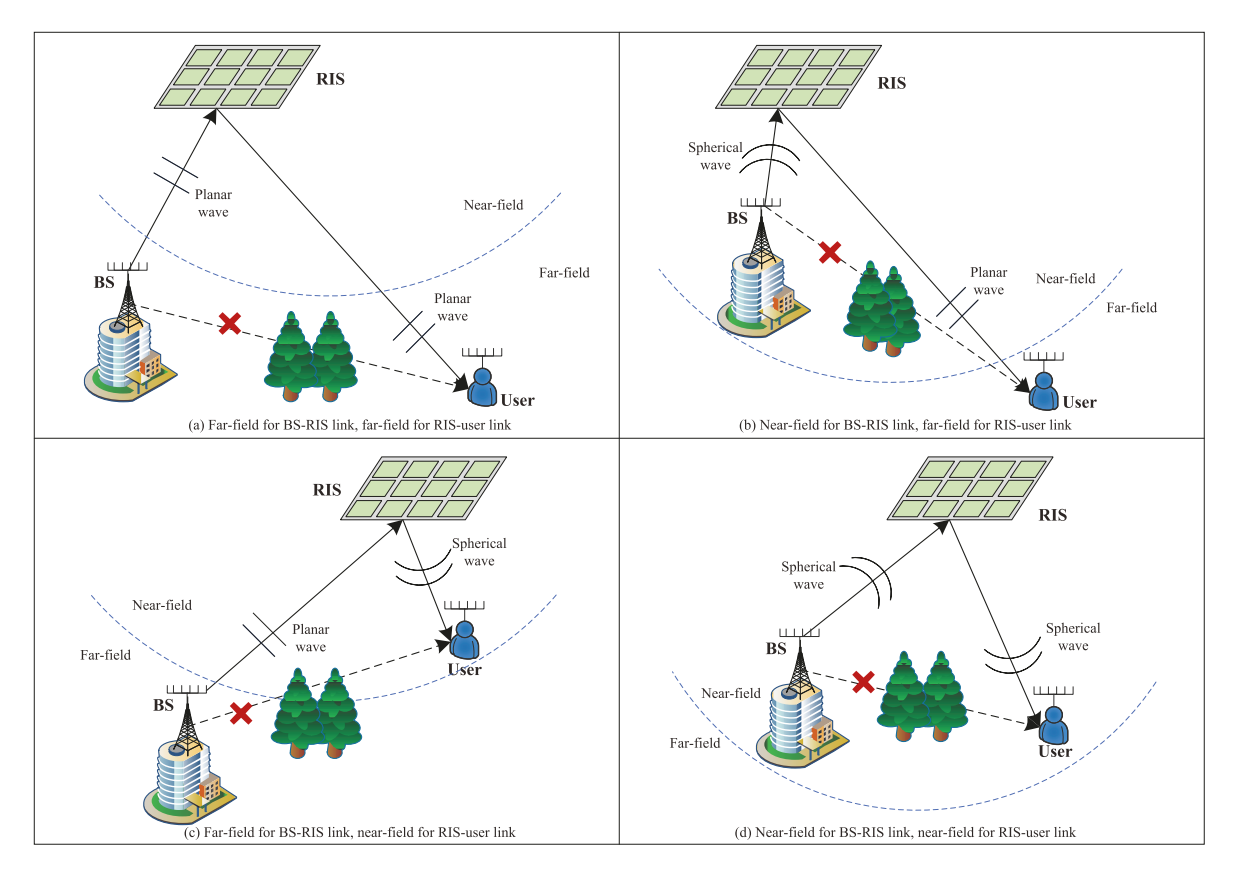


Fig. 1. Different channel models for RIS-assisted communication system.

TABLE I

COMPARISON BETWEEN THE FAR-FIELD AND NEAR-FIELD REGIONS IN RIS-ASSISTED SYSTEMS

	BS-RIS channel	RIS-user channel
Far-field	$r_{\mathrm{B,R}} > \frac{2(D_{\mathrm{B}} + D_{\mathrm{R}})^2}{\lambda_c}$	$r_{\mathrm{R,U}} > \frac{2(D_{\mathrm{R}} + D_{\mathrm{U}})^2}{\lambda_c}$
Near-field	$r_{\mathrm{B,R}} \le \frac{2(D_{\mathrm{B}} + D_{\mathrm{R}})^2}{\lambda_c}$	$r_{\mathrm{R,U}} \le \frac{2(D_{\mathrm{R}} + D_{\mathrm{U}})^2}{\lambda_c}$
Boundary $(d = \lambda_c/2)$	$\frac{\left[ (N_{\rm B} - 1) + \sqrt{(M_x - 1)^2 + \left(M_y - 1\right)^2} \right]^2 \lambda_c}{2}$	$\frac{\left[ (N_{\rm U} - 1) + \sqrt{(M_x - 1)^2 + (M_y - 1)^2} \right]^2 \lambda_c}{2}$

# A. Channel Model

In order to explore the differences among the four channel scenarios in terms of signal model, beam design, transmission performance, etc., we first provide mathematical descriptions of the models below. More specifically, we will first present the far-field model for the BS-RIS and RIS-user channels, then give the near-field model for the BS-RIS and RIS-user channels, and finally obtain the cascaded channel models for the four channel scenarios mentioned above.

1) Far-Field Channel Model: When the far-field channel model is considered, the channel between the BS and RIS is characterized by the Saleh-Valenzuela channel model [36], given by

$$\mathbf{G}_{\mathrm{B,R}}^{\mathrm{far}} = \sqrt{\frac{MN_{\mathrm{B}}}{L_{\mathrm{B}}}} \sum_{l=0}^{L_{\mathrm{B}}-1} \beta_{l} \mathbf{a}_{\mathrm{R}} \left(\alpha_{l}^{\mathrm{A}}, \varphi_{l}^{\mathrm{A}}\right) \mathbf{a}_{\mathrm{B}}^{H} \left(\alpha_{l}^{\mathrm{D}}\right), \quad (1)$$

where  $L_{\rm B}$  is the number of paths between the BS and RIS,  $\beta_0$  represents the complex gain of the line-of-sight (LoS) component,  $\beta_l$  ( $1 \le l \le L_{\rm B} - 1$ ) denotes the complex gain of

the l-th non-line-of-sight (NLoS) path [37],  $\alpha_l^{\rm A}$  and  $\varphi_l^{\rm A}$  denote the azimuth and elevation AoA associated with the RIS,  $\alpha_l^{\rm D}$  denotes the AoD associated with the BS, and  ${\bf a}_{\rm R}\left(\alpha_l^{\rm A},\varphi_l^{\rm A}\right)$  and  ${\bf a}_{\rm B}\left(\alpha_l^{\rm D}\right)$  are the array response vectors associated with the RIS and the BS, respectively.

For a UPA with  $M_x$  and  $M_y$  elements  $(M_x M_y = M)$  on the horizontal and the vertical axes respectively, the RIS array response vector is given by

$$\mathbf{a}_{\mathrm{R}}(\alpha,\varphi) = \frac{1}{\sqrt{M}} \left[ 1, \cdots, e^{-j\frac{2\pi d}{\lambda_{c}}(M_{x}-1)\sin\alpha\sin\varphi} \right]^{T}$$

$$\otimes \left[ 1, \cdots, e^{-j\frac{2\pi d}{\lambda_{c}}(M_{y}-1)\cos\varphi} \right]^{T}, \tag{2}$$

where  $0 \le x \le (M_x - 1)$  and  $0 \le y \le (M_y - 1)$ , and  $\otimes$  is the Kronecker product. For the ULA with  $N_B$  elements at the BS, the array response vector is expressed as [38]

$$\mathbf{a}_{\mathrm{B}}\left(\alpha\right) = \frac{1}{\sqrt{N_{\mathrm{B}}}} \left[1, \cdots, e^{-j(N_{\mathrm{B}}-1)\frac{2\pi d}{\lambda_{c}}\sin\alpha}\right]^{T}, \quad (3)$$

where  $0 \le n_b \le (N_B - 1)$ . Since the response vector of a ULA is constant in the elevation domain, we omit the parameter  $\varphi$  in the response vector of the BS in (3).

Similarly, the channel between the RIS and user in the farfield region is given by

$$\mathbf{G}_{\mathrm{R,U}}^{\mathrm{far}} = \sqrt{\frac{MN_{\mathrm{U}}}{L_{\mathrm{U}}}} \sum_{l=0}^{L_{\mathrm{U}}-1} \beta_{l} \mathbf{a}_{\mathrm{U}} \left(\alpha_{l}^{\mathrm{A}}\right) \mathbf{a}_{\mathrm{R}}^{H} \left(\alpha_{l}^{\mathrm{D}}, \varphi_{l}^{\mathrm{D}}\right), \quad (4)$$

where  $L_{\rm U}$  is the number of paths between the RIS and user,  $\alpha_l^{\rm A}$  denotes the azimuth AoA associated with the user,  $\alpha_l^{\rm D}$  and  $\varphi_l^{\rm D}$  denote the azimuth and elevation AoD associated with the RIS respectively, and the array response vectors  $\mathbf{a}_{\rm R}\left(\alpha_l^{\rm D},\varphi_l^{\rm D}\right)$  and  $\mathbf{a}_{\rm U}\left(\alpha_l^{\rm A}\right)$  can be generated similarly to (2) and (3).

Remark 1: Assume that the number of RIS elements is far larger than the number of BS and user antennas. When the far-field channel model is considered (no matter whether the BS-RIS link or the RIS-user link follows the far-field model), the rank r of the cascaded BS-RIS-user channel satisfies  $r \leq \min\{L_{\rm B}, L_{\rm U}\}$ , and we say that the channel has r degrees of freedom (DoFs) [39]. Thus, the dimension of the transmitted signal vector should satisfy  $q \leq r \leq \min\{L_{\rm B}, L_{\rm U}\}$ . When environmental scattering is absent and no NLoS paths are present, the rank of the cascaded channel is 1.

2) Near-Field Channel Model: For communications in the near-field domain, we consider a three-dimensional topology. In FFC, the signal propagation paths from transmitters to receivers can be regarded as parallel to each other if they share the same AoA. However, in NFC, the angle distribution is also related to the distance between specific points of transmitters and receivers. Assume that all the BS antennas are located on the x-axis, where the coordinate of the midpoint of the BS array is denoted as (0,0,0). Thus, the coordinate of the  $n_b$ -th antenna at the BS can be denoted as

$$\mathbf{q}_{\mathrm{B}}(n_b) = (\tilde{n}_b d, 0, 0), \tag{5}$$

where  $\tilde{n}_b = n_b - \frac{N_{\rm B}-1}{2}$ .

Similarly, assume that all of the user antennas are parallel to the x-axis, where the coordinate of the midpoint of the user array is  $(x_{\rm U},y_{\rm U},z_{\rm U})$ . Thus, the location of  $n_u$ -th antenna at the user can be denoted as

$$\mathbf{q}_{\mathrm{U}}(n_{u}) = (x_{\mathrm{U}} + \tilde{n}_{u}d, y_{\mathrm{U}}, z_{\mathrm{U}}), \qquad (6)$$

where  $\tilde{n}_u = n_u - \frac{N_{\rm U} - 1}{2}$ .

Assume that all elements of the RIS are parallel to the XY-plane. Denote the coordinate of the midpoint of the RIS as  $(x_{\rm R},y_{\rm R},z_{\rm R})$ . Thus, the coordinate of the  $(m_x,m_y)$ -th element of the RIS can be expressed as

$$\mathbf{q}_{\mathrm{R}}(m_x, m_y) = (x_{\mathrm{R}} + \tilde{m}_x d, y_{\mathrm{R}} + \tilde{m}_y d, z_{\mathrm{R}}), \qquad (7)$$

where  $\tilde{m}_x = m_x - \frac{M_x - 1}{2}$  and  $\tilde{m}_y = m_y - \frac{M_y - 1}{2}$ . Further, assume that the location and topology of the RIS are known.

Based on the above geometry, the LoS link for the near-field channel between BS and RIS can be modeled as [40]

$$\mathbf{G}_{\mathrm{B,R}}^{\mathrm{near}} = \left[ \mathbf{g}_{\mathrm{B,R}}^{1}, \cdots, \mathbf{g}_{\mathrm{B,R}}^{m_{xy}}, \cdots, \mathbf{g}_{\mathrm{B,R}}^{M} \right]^{T}, \tag{8}$$

where  $\mathbf{g}_{\mathrm{B,R}}^{m_{xy}} = \left[\kappa_{m_{xy},1}e^{-j\frac{2\pi}{\lambda_c}d_{m_{xy},1}^{\mathrm{B}}},\cdots,\kappa_{m_{xy},N_{\mathrm{B}}}e^{-j\frac{2\pi}{\lambda_c}d_{m_{xy},N_{\mathrm{B}}}^{\mathrm{B}}}\right]^{T}$  and  $\kappa_{m_{xy},n_{b}} \propto \frac{1}{d_{m_{xy},n_{b}}^{\mathrm{B}}}$  denotes the free-space large-scale path loss between the  $n_{b}$ -th antenna of the BS and the  $(m_{x},m_{y})$ -th element of the RIS. The distance between the  $n_{b}$ -th antenna of the BS and the  $(m_{x},m_{y})$ -th element of the RIS is given by

$$d_{m_{xy},n_b}^{\mathrm{B}} = \|\mathbf{q}_{\mathrm{B}}(n_b) - \mathbf{q}_{\mathrm{R}}(m_x, m_y)\|_2,$$
 (9)

which can be expanded as

$$d_{m_{xy},n_{b}}^{B} = \sqrt{(x_{R} + \tilde{m}_{x}d - \tilde{n}_{b}d)^{2} + (y_{R} + \tilde{m}_{y}d)^{2} + z_{R}^{2}}$$

$$= \sqrt{r_{m_{xy}}^{B}{}^{2} + (\tilde{n}_{b}d)^{2} - 2\tilde{n}_{b}dr_{m_{xy}}^{B}\sin\alpha_{m_{xy}}^{B}\sin\varphi_{m_{xy}}^{B}}$$

$$\stackrel{(a)}{\approx} r_{m_{xy}}^{B} - \tilde{n}_{b}d\sin\alpha_{m_{xy}}^{B}\sin\varphi_{m_{xy}}^{B}$$

$$+ \frac{(\tilde{n}_{b}d)^{2}\left(1 - \sin^{2}\alpha_{m_{xy}}^{B}\sin^{2}\varphi_{m_{xy}}^{B}\right)}{2r_{m_{xy}}^{B}}, \qquad (10)$$

with  $r_{m_{xy}}^{\rm B}$  denoting the distance between (0,0,0) and the  $(m_x,m_y)$ -th element of the RIS,  $\alpha_{m_{xy}}^{\rm B}$ ,  $\varphi_{m_{xy}}^{\rm B}$  denoting the corresponding azimuth and elevation angle, respectively, and (a) is obtained based on the first-order Taylor expansion  $\sqrt{1+x}=1+\frac{1}{2}x-\frac{1}{8}x^2+\mathcal{O}\left(x^3\right)$ .

Similarly, the LoS near-field channel between the RIS and user can be modeled as

$$\mathbf{G}_{\mathrm{R,U}}^{\mathrm{near}} = \left[\mathbf{g}_{\mathrm{R,U}}^{1}, \cdots, \mathbf{g}_{\mathrm{R,U}}^{n_{u}}, \cdots, \mathbf{g}_{\mathrm{R,U}}^{N_{\mathrm{U}}}\right]^{T}, \tag{11}$$

where  $\mathbf{g}_{\mathrm{R,U}}^{n_u} = \left[\kappa_{n_u,1}e^{-j\frac{2\pi}{\lambda_c}d_{n_u,1}^{\mathrm{U}}},\cdots,\kappa_{n_u,M}e^{-j\frac{2\pi}{\lambda_c}d_{n_u,M}^{\mathrm{U}}}\right]^T$  and  $\kappa_{n_u,m_{xy}} \propto \frac{1}{d_{n_u,m_{xy}}^{\mathrm{U}}}$  denote the free-space large-scale path loss between the  $n_u$ -th antenna of the user and the  $(m_x,m_y)$ -th element of the RIS. The distance between the  $n_u$ -th antenna of the user and the  $(m_x,m_y)$ -th element of the RIS is given by

$$d_{n_{u},m_{xy}}^{U} = \|\mathbf{q}_{U}(n_{u}) - \mathbf{q}_{R}(m_{x},m_{y})\|_{2},$$
 (12)

which can be approximated as

$$d_{n_{u},m_{xy}}^{\mathrm{U}} \approx r_{m_{xy}}^{\mathrm{U}} - \tilde{n}_{u} d \sin \alpha_{m_{xy}}^{\mathrm{U}} \sin \varphi_{m_{xy}}^{\mathrm{U}} + \frac{(\tilde{n}_{u} d)^{2} \left(1 - \sin^{2} \alpha_{m_{xy}}^{\mathrm{U}} \sin^{2} \varphi_{m_{xy}}^{\mathrm{U}}\right)}{2r_{m_{xy}}^{\mathrm{U}}}, \quad (13)$$

with  $r_{m_{xy}}^{\rm U}$  denoting the distance between the midpoint of the user array and the  $(m_x,m_y)$ -th element of the RIS,  $\alpha_{m_{xy}}^{\rm U}$ ,  $\varphi_{m_{xy}}^{\rm U}$  denoting the corresponding azimuth and elevation angle, respectively.

Remark 2: When both the BS-RIS and RIS-user links are in the near-field region, the rank of the cascaded LoS channel is  $r = \min\{N_B, N_U, M\}$ , which will be much larger than 1 in the case of large-scale arrays, even in the absence of NLoS paths. Thus, one of the main advantages of near-field communications is that they possess higher DoFs and can support q(q > 1) data streams without relying on abundant

environmental scattering, thus providing enhanced DoF in RIS-aided NFC [43].

3) Cascaded Channel Model: Denote the phase-shift matrix of the RIS as  $\Theta = \mathrm{diag}\big(\phi_1,\cdots,\phi_m,\cdots,\phi_M\big)$ , with  $\phi_m = e^{-j\theta_m},\theta_m \in [0,2\pi)$  denoting the phase-shift coefficient of the m-th RIS element. Therefore, the cascaded channels of the four scenarios mentioned above can be expressed as

1) 
$$\mathbf{H}_{\mathrm{FF}} = \mathbf{G}_{\mathrm{R,U}}^{\mathrm{far}} \mathbf{\Theta} \mathbf{G}_{\mathrm{B,R}}^{\mathrm{far}},$$
 (14a)

2) 
$$\mathbf{H}_{NF} = \mathbf{G}_{R II}^{far} \mathbf{\Theta} \mathbf{G}_{R R}^{near},$$
 (14b)

3) 
$$\mathbf{H}_{FN} = \mathbf{G}_{R,U}^{near} \mathbf{\Theta} \mathbf{G}_{B,R}^{far},$$
 (14c)

4) 
$$\mathbf{H}_{\mathrm{NN}} = \mathbf{G}_{\mathrm{R.U}}^{\mathrm{near}} \mathbf{\Theta} \mathbf{G}_{\mathrm{B.R}}^{\mathrm{near}}$$
. (14d)

# B. Signal Model

We assume that fully-digital beamforming is adopted at the BS, and thus the BS transmitted signal is given by

$$\mathbf{s} = \mathbf{W}\mathbf{x},\tag{15}$$

where  $\mathbf{x} \in \mathbb{C}^{q \times 1}$  is the symbol vector, satisfying  $\mathbb{E}\left[\mathbf{x}\mathbf{x}^H\right] = \mathbf{I}_q$ , and  $\mathbf{W} \in \mathbb{C}^{N_{\mathrm{B}} \times q}$  is the beamforming matrix.

Assuming the receiver adopts a linear combiner, the received signal at the user is given by

$$y = U^H H W x + U^H n, \tag{16}$$

where  $\mathbf{U} \in \mathbb{C}^{N_{\mathrm{U}} \times q}$  is the combining matrix,  $\mathbf{H} \in \{\mathbf{H}_{\mathrm{FF}}, \mathbf{H}_{\mathrm{NF}}, \mathbf{H}_{\mathrm{FN}}, \mathbf{H}_{\mathrm{NN}}\}$  is the cascaded channel between the BS and the user based on the specific channel model, and  $\mathbf{n} \in \mathcal{CN}\left(\mathbf{0}, \sigma^2 \mathbf{I}_{N_{\mathrm{U}}}\right)$  is additive white Gaussian noise (AWGN).

The maximum achievable data rate (bits/s/Hz) for the user is given by

$$R(\mathbf{W}, \mathbf{\Theta}) = \log_2 \left| \mathbf{I}_{N_{\text{U}}} + \mathbf{H} \mathbf{W} \mathbf{W}^H \mathbf{H}^H \sigma^{-2} \right|,$$
 (17)

where |X| represents the determinant of the matrix X.

Remark 3: Equation (17) characterizes the maximum achievable rate when the optimal combiner at the user, denoted as  $\mathbf{U}_{\mathrm{opt}}$ , is adopted. Given  $\{\mathbf{W}, \boldsymbol{\Theta}\}$ , closed-form solutions for  $\mathbf{U}_{\mathrm{opt}}$  can be obtained, as detailed in the sequel.

#### III. RIS CODEBOOK DESIGN

The precise design of the RIS coefficient matrix requires accurate channel information, which is difficult to obtain due to the passivity of RISs. Therefore, in this article, we consider exploiting beam training, which can perform channel estimation and RIS coefficient optimization simultaneously. To begin with, in this section, we will first design codebooks for different channel models. Based on the information contained in the received signals, angular-domain and distance-based codebooks are designed for FF and NN models respectively, while a combined angular-distance (AD) codebook is designed for NF and FN models. Each column in the designed codebook corresponds to one candidate RIS passive beamforming vector.

 $^{1}$ In this article, we mainly consider the transmission of LoS path to compare the performance of far- and near-field communications in a non-scattering environment, i.e.,  $L_{B}=L_{U}=1$ . This setting is to demonstrate that NFC can support multiple data streams and have higher DoFs in the same non-scattering environments. In this case, only a single RF chain is required in FFC due to the low rank of far-field channels [41], and 2q RF chains are required in NFC to achieve the same performance as fully-digital beamforming [42].

#### A. Angular-Domain Codebook for FF

In this subsection, we consider an angular-domain codebook that is universal in the far-field domain. Generally, existing RIS codebooks for FF channel models aim at aligning the beam to the strongest propagation path to maximize the beamforming gain. Ignoring weak paths, the signal at the user can be written as

$$\mathbf{y}_{\mathrm{FF}} = \beta_0' \mathbf{U}^H \mathbf{a}_{\mathrm{U}} \left( \alpha_0^{\mathrm{A}} \right) \mathbf{a}_{\mathrm{R}}^H \left( \alpha_0^{\mathrm{D}}, \varphi_0^{\mathrm{D}} \right) \mathrm{diag} \left( \boldsymbol{\phi} \right) \\ \times \mathbf{a}_{\mathrm{R}} \left( \alpha_0^{\mathrm{A}}, \varphi_0^{\mathrm{A}} \right) \mathbf{a}_{\mathrm{B}}^H \left( \alpha_0^{\mathrm{D}} \right) \mathbf{W} \mathbf{x} + \mathbf{U}^H \mathbf{n}, \quad (18)$$

where  ${\beta_0}'$  denotes the complex gain of the cascaded LoS channel. By substituting the array response vectors  ${\bf a}_{\rm R}\left(\alpha_0^{\rm D},\varphi_0^{\rm D}\right)$  and  ${\bf a}_{\rm R}\left(\alpha_0^{\rm A},\varphi_0^{\rm A}\right)$  into (18), the user's signal can be reformulated as

$$\mathbf{y}_{\mathrm{FF}} = \beta_0' \mathbf{U}^H \mathbf{a}_{\mathrm{U}} \left( \alpha_0^{\mathrm{A}} \right)$$

$$\times \sum_{n=1}^{M} e^{-j \left( \theta_m + \nu_m^{\mathrm{A}} - \nu_m^{\mathrm{D}} \right)} \mathbf{a}_{\mathrm{B}}^H \left( \alpha_0^{\mathrm{D}} \right) \mathbf{W} \mathbf{x} + \mathbf{U}^H \mathbf{n}, \quad (19)$$

where  $\nu_m^{\rm A}=\frac{2\pi d}{\lambda_c}\left[(m_x-1)\sin\alpha_0^{\rm A}\sin\varphi_0^{\rm A}+(m_y-1)\cos\varphi_0^{\rm A}\right]$  and  $\nu_m^{\rm D}=\frac{2\pi d}{\lambda_c}\left[(m_x-1)\sin\alpha_0^{\rm D}\sin\varphi_0^{\rm D}+(m_y-1)\cos\varphi_0^{\rm D}\right].$  Thus, the optimal RIS phase-shift coefficients are  $\theta_m=\nu_m^{\rm D}-\nu_m^{\rm A}.$  All candidate angle pairs on the beam grid should be considered when accurate channel state information is unavailable, which is one of the primary principles for far-field codebook design.

Assume that **U** and **W** have already been designed to align with the strongest path [23], and focus on coefficient optimization at RIS for codebook design. **U** and **W** can be designed with the channel information obtained through beam training, and we will show how **U** and **W** can be obtained later. Thus, the RIS codebook for the FF channel model can be designed as [32], [34]

$$\mathcal{F}_{\text{FF}} = \left[ \mathbf{b} \left( \beta_1, \delta_1 \right), \cdots, \mathbf{b} \left( \beta_{m_x}, \delta_{m_y} \right), \cdots, \mathbf{b} \left( \beta_{M_x}, \delta_{M_y} \right) \right]^*, \tag{20}$$

where  $\beta_{m_x}=\frac{2m_x-M_x-1}{M_x}$  with  $m_x=1,\cdots,M_x$ ,  $\delta_{m_y}=\frac{2m_y-M_y-1}{M_y}$  with  $m_y=1,\cdots,M_y$ , and  $\mathbf{b}\left(\beta,\delta\right)$  is the following far-field steering vector

$$\mathbf{b}(\beta, \delta) = \left[1, \cdots, e^{-j\frac{2\pi d}{\lambda_c}(M_x - 1)\beta\delta}\right]^T$$

$$\otimes \left[1, \cdots, e^{-j\frac{2\pi d}{\lambda_c}(M_y - 1)\delta}\right]^T. \quad (21)$$

Each column of  $\mathcal{F}_{\mathrm{FF}}$  is a candidate beam codeword for the RIS in the far-field domain. This angular-domain codebook design makes full use of the angular information of the far-field paths.

# B. Distance-Based Codebook Design for NN

Angular-only far-field codebooks are not applicable to near-field channels, even if only one or the other of the BS-RIS and RIS-user links is in the near-field domain because both distance and angular information are embedded in the received signal. Therefore, novel codebooks are required to match the channels in the near-field region. When both the BS-RIS link and RIS-user link are in the near-field domain, the combined

signal at the user is given by (22), shown at the bottom of the page, where  $\nu_{n_u,m,n_b}=\frac{2\pi}{\lambda_c}\left(d^{\rm U}_{n_u,m}+d^{\rm B}_{m,n_b}\right)$ , determined by the sum of the distances from the BS to RIS and from the RIS to the user.

Define the following array steering vector related to the distance

$$\boldsymbol{f}(x,y,z) = \exp\left[-j\frac{2\pi}{\lambda_c} \left(r_{1,1},\dots,r_{m_x,m_y},\dots,r_{M_x,M_y}\right)\right]^T,$$
(23)

where (x,y,z) denotes the coordinate of the BS or the user, and  $r_{m_x,m_y} = \|(x,y,z),\mathbf{q}_{\mathrm{R}}(m_x,m_y)\|_2$ . Generally, the height of the BS or the user is constant. Therefore, for the design of the near-field codebooks, we mainly consider the exploration of x and y, and the z component in f(x,y,z) will be omitted hereafter.

Definition 1:  $\{\mathbf{x}_1, \dots, \mathbf{x}_M\}$  and  $\{\mathbf{y}_1, \dots, \mathbf{y}_N\}$  are two sets of vectors with the same dimension. The  $\star$  operator is defined as follows for vectors of equal dimensions:

$$[\mathbf{x}_{1}, \cdots, \mathbf{x}_{M}] \star [\mathbf{y}_{1}, \cdots, \mathbf{y}_{N}]$$

$$= [\mathbf{x}_{1} \odot \mathbf{y}_{1}, \cdots, \mathbf{x}_{1} \odot \mathbf{y}_{N}, \cdots, \mathbf{x}_{M} \odot \mathbf{y}_{N}], \qquad (24)$$

where  $\odot$  denotes the Hadamard product.

We use a pair of coordinates to represent the rectangular sampling range on the XY-plane as  $(x_{\min}^k, y_{\min}^k)$  and  $(x_{\max}^k, y_{\max}^k)$ , where  $x_{\min}^k$   $(y_{\min}^k)$  and  $x_{\max}^k$   $(y_{\max}^k)$  are the minimum and the maximum x (y)-coordinate of the sampling points respectively, and  $k \in \{B, U\}$  indicates the BS or user. Denote the number of points sampled on the x-axis and y-axis as  $S_x$  and  $S_y$ , respectively. Taking the corresponding distance between the sampling points into account, the codebook at the RIS for the NN channel model is given by

$$\mathcal{F}_{\text{NN}} = \left[ \boldsymbol{f} \left( x_{1}^{\text{U}}, y_{1}^{\text{U}} \right), \cdots, \boldsymbol{f} \left( x_{s_{x}}^{\text{U}}, y_{s_{y}}^{\text{U}} \right), \cdots, \boldsymbol{f} \left( x_{S_{x}}^{\text{U}}, y_{S_{y}}^{\text{U}} \right) \right]^{*} \\
\star \left[ \boldsymbol{f} \left( x_{1}^{\text{B}}, y_{1}^{\text{B}} \right), \cdots, \boldsymbol{f} \left( x_{s_{x}}^{\text{B}}, y_{s_{y}}^{\text{B}} \right), \cdots, \boldsymbol{f} \left( x_{S_{x}}^{\text{B}}, y_{S_{y}}^{\text{B}} \right) \right]^{*},$$
(25)

where  $\boldsymbol{x}_{s_x}^k$  and  $\boldsymbol{y}_{s_x}^k$  are given by

$$x_{s_x}^k = x_{\min}^k + \left(s_x - \frac{1}{2}\right) \frac{x_{\max}^k - x_{\min}^k}{S_x}, \ s_x = 1, \dots, S_x,$$
 (26a)

$$y_{s_y}^k = y_{\min}^k + \left(s_y - \frac{1}{2}\right) \frac{y_{\max}^k - y_{\min}^k}{S_y}, \ s_y = 1, \dots, S_y.$$
 (26b)

The size of the codebook will increase with the number of sampling points in each direction, and the accuracy of the RIS beamforming will improve correspondingly.

#### C. Combined AD Codebook Design for Hybrid FFC & NFC

In this section, we consider hybrid cascaded channel models, where one side of the RIS is in the far-field and the other is in the near-field. As such, the link on one side of RIS only needs to consider angular information, while the link on the other side needs to consider both angular and distance information. Taking the FN channel model as an example, i.e., with the BS-RIS link in the far-field and the RIS-user link in the near-field, the received signal at the user is given by

$$\mathbf{y}_{\text{FN}} = \mathbf{U}^H \mathbf{G}_{\text{R,U}}^{\text{near}} \operatorname{diag}(\boldsymbol{\phi}) \mathbf{G}_{\text{B,R}}^{\text{far}} \mathbf{W} \mathbf{x} + \mathbf{U}^H \mathbf{n}.$$
 (27)

By substituting  $\mathbf{G}_{R,U}^{\mathrm{near}}$  in (11) and  $\mathbf{G}_{B,R}^{\mathrm{far}}$  in (1) into (27),  $\mathbf{y}_{\mathrm{FN}}$  can be expanded into the following form

$$\mathbf{y}_{\text{FN}} = \frac{\beta_0 \lambda_c}{4\pi \sqrt{M}} \mathbf{U}^H \left[ \sum_{m=1}^M \frac{1}{d_{1,m}^{\text{U}}} e^{-j\left(\theta_m + \nu_{1,m}^{\text{A}}\right)}, \cdots, \right]$$

$$\sum_{m=1}^M \frac{1}{d_{N_{\text{U}},m}^{\text{U}}} e^{-j\left(\theta_m + \nu_{N_{\text{U}},m}^{\text{A}}\right)} \mathbf{a}_{\text{B}}^H \left(\alpha_0^{\text{D}}\right) \mathbf{W} \mathbf{x} + \mathbf{U}^H \mathbf{n},$$
(28)

where

$$\nu_{n_{u},m}^{A} = \frac{2\pi}{\lambda_{c}} \left[ (m_{x} - 1) d \sin \alpha_{0}^{A} \sin \varphi_{0}^{A} + (m_{y} - 1) d \cos \varphi_{0}^{A} + d_{n_{u},m}^{U} \right].$$
(29)

Similar to the assumptions above for FF channels, we assume that the transmit or receive beam related to the far-field link has been designed to align with the steering vector of the strongest path. That is to say,  $\mathbf{W}$  has been aligned to  $\mathbf{a}_{\mathrm{B}}^{H}\left(\alpha_{0}^{\mathrm{D}}\right)$  when designing the RIS codebook.

Considering the array response in both the distance and angular domains, we define the array steering vector as

$$\mathbf{c}(x,y,\beta,\delta) = \left[e^{-j\frac{2\pi}{\lambda_c}d_{1,1}}, \cdots, e^{-j\frac{2\pi}{\lambda_c}d_{M_x,M_y}}\right]^T$$

$$\odot \left\{ \left[1, \cdots, e^{-j\frac{2\pi d}{\lambda_c}(M_x - 1)\beta\delta}\right]^T$$

$$\otimes \left[1, \cdots, e^{-j\frac{2\pi d}{\lambda_c}(M_y - 1)\delta}\right]^T \right\}, \quad (30)$$

where  $d_{m_x,m_y} = \|(x,y,z), \mathbf{q}_{\mathrm{R}}(m_x,m_y)\|_2$  and z is assumed to be fixed and known.

$$\mathbf{y}_{\text{NN}} = \left(\frac{\lambda_{c}}{4\pi}\right)^{2} \mathbf{U}^{H} \begin{bmatrix} \sum_{m=1}^{M} \frac{1}{d_{1,m}^{\text{U}} d_{m,1}^{\text{B}}} e^{-j(\theta_{m} + \nu_{1,m,1})} & \cdots & \sum_{m=1}^{M} \frac{1}{d_{1,m}^{\text{U}} d_{m,N_{\text{B}}}^{\text{B}}} e^{-j(\theta_{m} + \nu_{1,m,N_{\text{b}}})} \\ \vdots & & \vdots & & \vdots \\ \sum_{m=1}^{M} \frac{1}{d_{n_{u},m}^{\text{U}} d_{m,1}^{\text{B}}} e^{-j(\theta_{m} + \nu_{n_{u},m,1})} & \cdots & \sum_{m=1}^{M} \frac{1}{d_{n_{u},m}^{\text{U}} d_{m,N_{\text{B}}}^{\text{B}}} e^{-j(\theta_{m} + \nu_{n_{u},m,N_{\text{B}}})} \\ \vdots & & & \vdots \\ \sum_{m=1}^{M} \frac{1}{d_{N_{\text{U}},m}^{\text{U}} d_{m,1}^{\text{B}}} e^{-j(\theta_{m} + \nu_{N_{\text{U}},m,1})} & \cdots & \sum_{m=1}^{M} \frac{1}{d_{N_{\text{U}},m}^{\text{U}} d_{m,N_{\text{B}}}^{\text{B}}} e^{-j(\theta_{m} + \nu_{N_{\text{U}},m,N_{\text{B}}})} \end{bmatrix} \mathbf{W} \mathbf{x} + \mathbf{U}^{H} \mathbf{n}, \quad (22)$$

A codebook design for hybrid cascaded channel models should cover not only the angular region of all possible signals, but their distances as well. Therefore, based on the received signal model given in (27), the codebook for hybrid cascaded channel models should be designed to include the following two components.

1) Angular-Domain Sweeping, Similar to FFC: To align the phase on the FFC side, the full angular range will be covered in the predesigned codebook. Therefore, the first component of the RIS codebook for hybrid cascaded channel models is

$$\mathcal{F}_{Hb}^{1} = \left[ \mathbf{b} \left( \beta_{1}, \delta_{1} \right), \cdots, \mathbf{b} \left( \beta_{m_{x}}, \delta_{m_{y}} \right), \cdots, \mathbf{b} \left( \beta_{M_{x}}, \delta_{M_{y}} \right) \right]^{*},$$
(31)

where 
$$\beta_{m_x}=\frac{2m_x-M_x-1}{M_x}$$
 with  $m_x=1,\cdots,M_x$ ,  $\delta_{m_y}=\frac{2m_y-M_y-1}{M_y}$  with  $m_y=1,\cdots,M_y$ .

2) Distance-Domain Sampling, Similar to NFC: For each

given angle pair  $\beta$  and  $\delta$ , all possible sampling points in the feasible range should be included to align the phase on the NFC side. Therefore, the second component of the RIS codebook for hybrid cascaded channel models is given by

$$\mathcal{F}_{Hb}^{2,k} = \left[ \boldsymbol{f} \left( x_1^k, y_1^k \right), \cdots, \boldsymbol{f} \left( x_{s_x}^k, y_{s_y}^k \right), \cdots, \boldsymbol{f} \left( x_{S_x}^k, y_{S_y}^k \right) \right]^*,$$
(32)

where  $x_{s_x}^k$  and  $y_{s_x}^k$ ,  $k \in \{B, U\}$ , are defined as in (26). In particular, k = B for the NF case, and k = U for the FN case.

Accordingly, the codebook at the RIS for hybrid cascaded channel models can be designed as

$$\mathcal{F}_{NF} = \mathcal{F}_{Hb}^{1} \star \mathcal{F}_{Hb}^{2,B}, \qquad (33a)$$
  
$$\mathcal{F}_{FN} = \mathcal{F}_{Hb}^{1} \star \mathcal{F}_{Hb}^{2,U}, \qquad (33b)$$

$$\mathcal{F}_{FN} = \mathcal{F}_{Hb}^1 \star \mathcal{F}_{Hb}^{2,U}, \tag{33b}$$

where  $\star$  is given in **Definition 1**.

# IV. AO-BASED ALGORITHM FOR MAXIMIZING RATE

We aim to maximize the achievable rate by jointly optimizing the combining matrix U at the user, the digital beamforming matrix W at the BS, and the reflecting coefficient matrix  $\Theta$  at the RIS. Suppose each passive beamforming vector at the RIS is selected from the predesigned codebooks. Therefore, the mathematical form of the optimization problem can be given as

(P) 
$$\max_{\mathbf{W}, \phi} R(\mathbf{W}, \operatorname{diag}(\phi)),$$
 (34a)

$$s.t. \|\mathbf{W}\|_F^2 \le P_{\text{max}},\tag{34b}$$

$$\phi \in \mathcal{F},$$
 (34c)

 $\in \{\mathcal{F}_{FF}, \mathcal{F}_{NF}, \mathcal{F}_{FN}, \mathcal{F}_{NN}\}$  in (34c) is the predesigned codebook based on the specific channel model.

To handle the highly-coupled non-convex problem in (34), we propose an alternating optimization algorithm in this section, where three sub-problems will be solved in an iterative manner. First, based on the predesigned codebooks, different beam training schemes will be proposed to perform the channel estimation and the RIS optimization for the specific

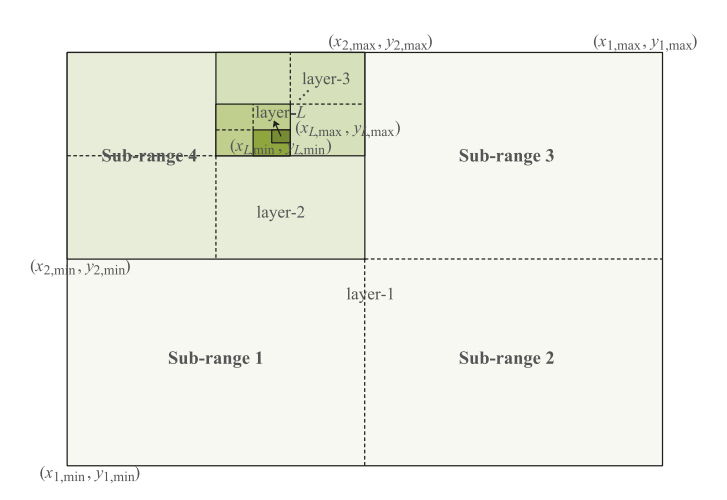


Fig. 2. Illustration for the proposed hierarchical beam training procedure.

channel models. Second, a closed-form solution for the receive combining matrix at the user is obtained. Finally, the active beamforming problem is solved by exploiting the relationship between the achievable rate and the mean square error. Details for solving these sub-problems are given in the following subsections.

### A. Beam Training Design for RIS

1) Angular-Domain Beam Sweeping for FF: The most direct method to perform beam training for this case is sweeping through all possible angles if the resulting training overhead is acceptable. The size of the FF codebook in (20) depends on the number of RIS reflecting elements. Based on the given angle pair  $\langle \beta_{m_x}, \delta_{m_y} \rangle$ , the corresponding codeword is  $\mathbf{b}\left(\beta_{m_x}, \delta_{m_y}\right)$ , and the achievable rate can be calculated as

$$R\left(\mathbf{W}, \operatorname{diag}\left(\mathbf{b}\left(\beta_{m_{-}}, \delta_{m_{-}}\right)\right)\right),$$
 (35)

with given beamforming matrix W. The optimal codeword is selected as the one that yields the maximum rate after sweeping through all candidate codewords in (20).

2) Hierarchical Beam Training Scheme for NN: From (25) and (26), we see that the NN codebook size is determined by the number of sampled points on the x-axis and y-axis. The beam training overhead can be reduced by reducing the codebook size (i.e., increasing the step size between the codebook samples), but this will reduce the performance of the beam training. In order to solve this problem, we design a hierarchical beam training approach that consists of several different levels of sub-codebooks. These sub-codebook levels are determined using different sampling ranges and sampling step sizes.

As illustrated in Fig. 2, we divide the sampling range parallel to the XY-plane into four sub-ranges in each layer, and find the range corresponding to the optimal codeword as the sampling range of the next layer. More particularly, in the l-th layer, the rectangular sampling range defined by the coordinate pairs  $\left(x_{\min}^k, y_{\min}^k\right)$  and  $\left(x_{\max}^k, y_{\max}^k\right)$ ,  $k \in \{\mathrm{B}, \mathrm{U}\}$ , is divided into the following four sub-ranges:

1) 
$$(x_{\min}^k, y_{\min}^k)$$
,  $(x_{\min}^k + x_{\Delta}, y_{\min}^k + y_{\Delta})$ , (36a)

2) 
$$(x_{\min}^k + x_{\Delta}, y_{\min}^k)$$
,  $(x_{\max}^k, y_{\min}^k + y_{\Delta})$ , (36b)

3) 
$$(x_{\min}^k + x_{\Delta}, y_{\min}^k + y_{\Delta}), (x_{\max}^k, y_{\max}^k),$$
 (36c)

4) 
$$(x_{\min}^k, y_{\min}^k + y_{\Delta}), (x_{\min}^k + x_{\Delta}, y_{\max}^k),$$
 (36d)

where  $x_{\Delta}=\frac{1}{2}\left[x_{\max}^k-x_{\min}^k\right]$  and  $y_{\Delta}=\frac{1}{2}\left[y_{\max}^k-y_{\min}^k\right]$ . Therefore, the sub-codebook for sub-range i of B and subrange j of U in the l-th layer, denoted by  $\mathcal{F}_{NN}(l,i,j), i,j =$ 1, 2, 3, 4, can be generated based on (25). Each column in  $\mathcal{F}_{\mathrm{NN}}\left(l,i,j\right)$  corresponds to a codeword  $\phi_{l,i,j,s}$ , with sdenoting the column index in sub-codebook  $\mathcal{F}_{NN}(l,i,j)$ . Based on the given beamforming matrix W and codeword  $\phi_{l,i,j,s}$ , the achievable rate can be calculated as

$$R\left(\mathbf{W}, \operatorname{diag}\left(\phi_{l,i,j,s}\right)\right).$$
 (37)

In fact, R can be calculated based on the corresponding received signal strength without accurate channel information.

By adopting the ES method, the optimal codeword can be obtained for the first layer, as well as the optimal sampling sub-range pair  $\langle i, j \rangle$ , which will be the sampling range in the next layer. This process is repeated until the maximum number of layers L is reached.

# Algorithm 1 Hierarchical Beam Training Scheme for NN

**Input:** sampling range  $x(y)_{\min(\max)}^k$ ,  $k \in \{B, U\}$ , number of sampled points in each layer  $S_x$  and  $S_y$ , maximum layer  $L_{\max}$ .

Output:  $\Theta_{opt}$ ,  $R_{opt}$ .

- 1: Initialization: l = 1,  $x(y)_{\min(\max)}^k(l) = x(y)_{\min(\max)}^k$ ,  $k \in \{B, U\}, R_{opt} = 0.$
- Divide the sampling ranges corresponding to both the BS and the user into four sub-ranges according to (36);
- Generate sub-codebooks  $\mathcal{F}_{NN}(l,i,j)$ , i,j=1,2,3,4, based on (25), where i is the sampling sub-range index for B and j is the sampling sub-range index for U;
- Based on the received signal strength, calculate the corresponding  $R(\mathbf{W}, \boldsymbol{\Theta})$  for each codeword;
- Find the maximum  $R(\mathbf{W}, \mathbf{\Theta})$ , the corresponding codeword  $\Theta_{\rm opt}$ , and the corresponding optimal sampling
- sub-range index pair  $\langle i,j \rangle$ ; Update  $x(y)_{\min(\max)}^{\mathrm{B}}$   $(l+1) = x(y)_{\min(\max)}^{\mathrm{B}}$  (l,i); Update  $x(y)_{\min(\max)}^{\mathrm{U}}$   $(l+1) = x(y)_{\min(\max)}^{\mathrm{U}}$  (l,j); 7:
- $l \leftarrow l + 1;$
- 10: until  $l = L_{\text{max}}$ .

The hierarchical beam training procedure is summarized in Algorithm 1. We define the size of the codebook as the number of candidate codewords, i.e., the number of column vectors. There are 16 sub-codebooks in each layer, and the size of each sub-codebook is  $(S_x S_y)^2$ . Therefore, with a given maximum number of training layers L, the training overhead can be calculated as  $16L(S_xS_y)^2$ . For the same sampling grid resolution and hence beam training accuracy, the training overhead of ES will be  $4^{L+1} (S_x S_y)^2$ .

3) Two-Stage Beam Training Scheme for FN and NF: The size of codebooks  $\mathcal{F}_{NF}$  and  $\mathcal{F}_{FN}$  is determined by the product of the number of RIS elements and the number of sample points, which can be extremely large especially for large RISs. Thus, while ES is a straightforward way to find the optimal codeword from the predefined codebooks, the training overhead and consumed time can be unacceptable. We therefore propose a two-stage beam training scheme for the FN and NF channel models. Specifically, all candidate angles are swept through in stage one, and the distance is determined in stage two based on the selected direction. The details are given as follows.

Stage 1: Angular-domain beam sweeping: In the first stage, we aim to find the optimal beamforming angle based on the far-field codebook given in (20), with the objective of maximizing the achievable rate in (17). All sampled angles will be swept through in this stage, and the one yielding the maximum achievable rate will be selected. Therefore, the selected indices in the angular-domain sweeping stage can be expressed mathematically as

$$\langle m_x, m_y \rangle_{\text{opt}}$$
  
=  $\operatorname{argmax} \left\{ \mathbf{b} \left( \beta_{m_x}, \delta_{m_y} \right) \in \mathcal{F}_{\text{FF}} \left| R \left( \mathbf{W}, \mathbf{\Theta}_{m_x, m_y} \right) \right. \right\},$  (38)

where  $\Theta_{m_x,m_y} = \operatorname{diag}\left(\mathbf{b}\left(\beta_{m_x},\delta_{m_y}\right)\right)$ . Denote the optimal index pair as  $\langle m'_x, m'_y \rangle$ .

Stage 2: Distance-domain sampling: In NFC, the beam can be designed to point at a particular location, rather than just a specific angle. Thus, in the second stage, we aim to determine the optimal focusing point for the optimal direction. With a given angle pair  $\langle m'_x, m'_y \rangle$ , the selected sampling point in the distance domain can be determined by

$$\left\langle x_{s_{x}}^{k}, y_{s_{y}}^{k} \right\rangle_{\text{opt}} = \operatorname{argmax} \left\{ \left( x_{s_{x}}^{k}, y_{s_{y}}^{k} \right) \in \mathcal{D}_{k} \middle| R\left( \mathbf{W}, \mathbf{\Theta}_{x_{s_{x}}^{k}, y_{s_{y}}^{k}} \right) \right\}, \quad (39)$$

where  $\mathcal{D}_k$  is the sampling range for  $k, k \in \{\mathrm{B}, \mathrm{U}\}$ , and  $\Theta_{x_{s_x}^k, y_{s_y}^k} = \mathrm{diag}\left(\mathbf{c}\left(x_{s_x}^k, y_{s_y}^k, \beta_{m_x'}, \delta_{m_y'}\right)\right)$ . Similar to the analysis in Section IV-A2, we adopt a

hierarchical beam training scheme in this stage to strike a balance between the training overhead and accuracy. Thus, the two-stage beam training procedure is summarized in **Algorithm 2.** The overhead of the proposed two-stage beam training scheme is  $M + 4LS_xS_y$ , while that of the ES method is  $M \times 4LS_xS_y$ .

Remark 4: The proposed beam training algorithms can be easily extended to scenarios with multiple users by dividing the RIS into multiple sub-surfaces, where each sub-surface implements the proposed beam training schemes to realize beam alignment for each user.

# B. Closed-Form Solution for U

With the estimated channel information acquired through the beam training, we can perform the BS beamforming and the user combining design. Although the combining matrix

# **Algorithm 2** Two-Stage Beam Training Scheme for Hybrid Cascaded Channel Models

**Input:**  $M_x$ ,  $M_y$ , sampling range  $x(y)_{\min(\max)}^k$ ,  $k \in \{B, U\}$ , number of sampled points in each layer  $S_x$  and  $S_y$ , maximum layer  $L_{\max}$ .

```
Output: \Theta_{opt}, R_{opt}.
 1: Initialization: m_x = 1, m_y = 1, R_{\text{opt}} = 0.
 3: Generate sub-codebook \mathcal{F}_{Hb}^1 based on (31);
 4: repeat
 5:
           repeat
               if R\left(\mathbf{W}, \mathbf{\Theta}_{m_x, m_y}\right) > R_{\mathrm{opt}} then R_{\mathrm{opt}} = R\left(\mathbf{W}, \mathbf{\Theta}_{m_x, m_y}\right); \langle m_x, m_y \rangle_{\mathrm{opt}} = \langle m_x, m_y \rangle;
 6:
 7:
 8:
 9:
               m_x \leftarrow m_x + 1;
10:
           until m_x = M_x;
11:
           m_y \leftarrow m_y + 1.
12:
13: until m_y = M_y;
14: Stage 2:
15: repeat
```

- 16: Divide the sampling ranges corresponding to the BS (NF Case) or the user (FN Case) into four sub-ranges according to (36);
- 17: Generate sub-codebooks  $\mathcal{F}_{\mathrm{Hy}}^2(l,i)$ , i=1,2,3,4, based on (32), where i is the sampling sub-range index for B (NF Case) or U (FN Case);
- 18: Generate  $\mathcal{F}_{\mathrm{NF}/\mathrm{FN}} = \left\{\mathcal{F}_{\mathrm{Hb}}^{1}\right\}_{\langle m_{x}, m_{y} \rangle_{\mathrm{opt}}} \star \mathcal{F}_{\mathrm{Hb}}^{2,k};$ 19: Based on the received signal strength, calculate the
- 19: Based on the received signal strength, calculate the corresponding  $R\left(\mathbf{W}, \mathbf{\Theta}_{x_{s_x}^k, y_{s_y}^k}\right)$  for each codeword;
- 20: Find the maximum  $R\left(\mathbf{W}, \mathbf{\Theta}_{x_{s_x}^k, y_{s_y}^k}\right)$ , the corresponding codeword  $\mathbf{\Theta}_{\mathrm{opt}}$ , and the corresponding optimal sampling sub-range index i;

```
21: Update x(y)_{\min(\max)}^k (l+1) = x(y)_{\min(\max)}^k (l,i);
22: l \leftarrow l+1;
23: until l = L_{\max}.
```

U is not present in the objective function (17), it will have an impact on the BS beamforming design and the achievable rate. Therefore, we derive the optimal combining matrix U at the user below. The principle of combining matrix design is to recover the original transmitted signals, which can be transformed into a mean square error (MSE) minimization problem. The MSE matrix of the user is given by

$$\mathbf{E} = \mathbb{E}\left[ (\mathbf{y} - \mathbf{x}) (\mathbf{y} - \mathbf{x})^{H} \right]$$

$$= (\mathbf{U}^{H} \mathbf{H} \mathbf{W} - \mathbf{I}_{q}) (\mathbf{U}^{H} \mathbf{H} \mathbf{W} - \mathbf{I}_{q})^{H} + \sigma^{2} \mathbf{U}^{H} \mathbf{U}, \quad (40)$$

and thus the mathematical form of the combining matrix optimization problem can be written as

(P1) 
$$\min_{\mathbf{U}} \operatorname{Tr}(\mathbf{E})$$
. (41)

With given **W** and  $\Theta$ , the optimal solution **U** of problem (41) can be obtained by solving  $\partial \text{Tr}(\mathbf{E})/\partial \mathbf{U} = \mathbf{0}$ , where  $\frac{\partial Tr(\mathbf{E})}{\partial \mathbf{U}} = 2 \left(\mathbf{H}\mathbf{W}\mathbf{W}^H\mathbf{H}^H + \sigma^2\mathbf{I}_{N_{\mathrm{U}}}\right)\mathbf{U} - 2\mathbf{H}\mathbf{W}$ . After

some simple derivations, the optimal combining matrix  ${\bf U}$  is found to be

$$\mathbf{U}_{\text{opt}} = \left(\mathbf{H}\mathbf{W}\mathbf{W}^H\mathbf{H}^H + \sigma^2\mathbf{I}_{N_{\text{U}}}\right)^{-1}\mathbf{H}\mathbf{W}, \quad (42)$$

which is necessary for the optimal value of W to achieve the maximum of (17).

### C. Active Beamforming Matrix Optimization

To solve the transmit beamforming optimization problem, we introduce an auxiliary matrix  $\mathbf{F} \succeq 0$ , and reformulate the original optimization as follows by exploiting the relationship between the achievable rate and the MSE [44]

$$(P') \max_{\mathbf{F}, \mathbf{W}, \boldsymbol{\phi}} f(\mathbf{F}, \mathbf{W}, \boldsymbol{\phi}),$$

$$s.t. (34b), (34c), \tag{43}$$

where  $f(\mathbf{F}, \mathbf{W}, \boldsymbol{\phi})$  is given by

$$f(\mathbf{F}, \mathbf{W}, \boldsymbol{\phi}) = \log |\mathbf{F}| - \text{Tr}(\mathbf{F}\mathbf{E}).$$
 (44)

The optimal **F** of problem (43) can be obtained by solving  $\partial f/\partial \mathbf{F} = \mathbf{0}$ , which is given by  $\mathbf{F} = \mathbf{E}^{-1}$ . With given **F**, **U** and  $\phi$ , the beamforming optimization problem can be expressed by substituting **E** into (44) and removing the constant terms:

(P2) 
$$\min_{\mathbf{W}} \operatorname{Tr} \left( \mathbf{W}^H \mathbf{H}^H \mathbf{U} \mathbf{F} \mathbf{U}^H \mathbf{H} \mathbf{W} \right) - 2 \operatorname{Tr} \left( \Re \left( \mathbf{F} \mathbf{U}^H \mathbf{H} \mathbf{W} \right) \right)$$
  
s.t. (34b), (45)

which is a convex optimization problem and its optimal solution can be obtained using standard methods.

# D. Overall Algorithm

The overall alternating optimization algorithm for maximizing the achievable rate is summarized in **Algorithm 3**, where the optimal solutions in each iteration are the inputs for the next iteration. First, with given  $\mathbf{U}^{(t)}$  and  $\mathbf{\Theta}^{(t)}$  at the t-th iteration, the optimal  $\Theta^{(t+1)}$  can be obtained by carrying out the beam training scheme based on Algorithm 2 or Algorithm 1. The estimated channel information can also be obtained in this step. Then, with given  $\Theta^{(t+1)}$  and  $\mathbf{W}^{(t)}$ , we calculate and update the combining matrix  $U^{(t+1)}$  according to (42). Although U is not included in the expression of the objective function in (17), it will serve as input for the next step in solving W. Last, with given  $U^{(t+1)}$ ,  $\Theta^{(t+1)}$  and  $W^{(t)}$ , we first obtain the reformulated objective function by substituting  $\mathbf{E}^{(t)}$ in (40) into (44), and then obtain the optimized beamforming matrix  $\mathbf{W}^{(t+1)}$  by solving problem (45). This process is repeated until a maximum number of iterations is reached or the convergence condition is satisfied. The proposed algorithm is summarized in Fig. 3.

The computational complexity of the beam training mainly comes from sorting, which requires  $\mathcal{O}(M)$  operations for angular-domain beam sweeping,  $\mathcal{O}\left(16L\left(S_xS_y\right)^2\right)$  operations for the hierarchical beam training scheme, and  $\mathcal{O}\left(M+4LS_xS_y\right)$  operations for the two-stage beam training algorithm. Solving problem (P1) for the combining matrix involves matrix inversion, leading to a computational

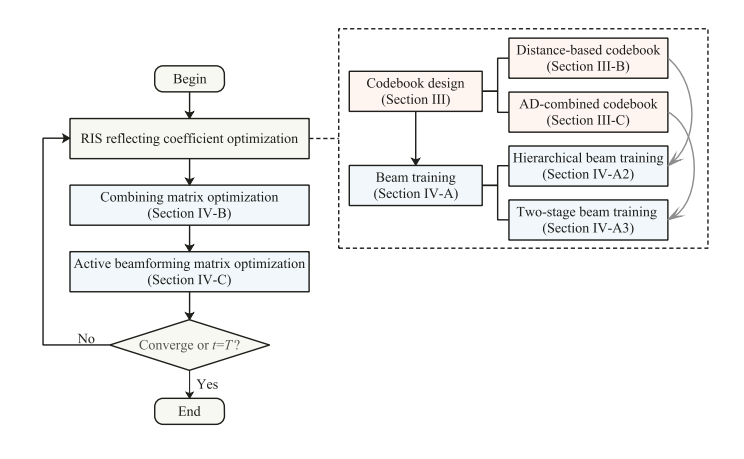


Fig. 3. Illustration for the proposed algorithm.

complexity of  $\mathcal{O}\left(N_{\mathrm{U}}^3\right)$  [45]. According to [46], the worst-case complexity for solving problem (P2) is  $\mathcal{O}\left(q^3N_{\mathrm{B}}^3\right)$  using efficient interior-point methods. Thus, the overall computational complexity of the proposed algorithm is  $\mathcal{O}\left(I_3\left(M+q^3N_{\mathrm{B}}^3+N_{\mathrm{U}}^3\right)\right)$  for FF with angular-domain beam sweeping,  $\mathcal{O}\left(I_3\left(16L\left(S_xS_y+q^3N_{\mathrm{B}}^3+N_{\mathrm{U}}^3\right)\right)\right)$  for NN with hierarchical beam training, and  $\mathcal{O}\left(I_3\left(M+4LS_xS_y+q^3N_{\mathrm{B}}^3+N_{\mathrm{U}}^3\right)\right)$  for NF and FN with two-stage beam training, with  $I_3$  representing the number of iterations required for the convergence of **Algorithm 3**.

**Algorithm 3** Alternating Optimization-Based Algorithm for Maximizing Achievable Rate

**Input:**  $R(\mathbf{W}, \mathbf{\Theta})$ , maximum iteration times T, convergence threshold  $\zeta$ .

Output:  $U_{\rm opt},\,\Theta_{\rm opt},\,W_{\rm opt}.$ 

- 1: Initialization: t = 0,  $\mathbf{U}^{(t)}$ ,  $\mathbf{\Theta}^{(t)}$ ,  $\mathbf{W}^{(t)}$ ,  $R^{(t)}$  ( $\mathbf{W}$ ,  $\mathbf{\Theta}$ ).
- 2: while  $t \leq T$  and  $\Gamma \geq \zeta$  do
- 3: For given  $U^{(t)}$  and  $W^{(t)}$ , perform beam training based on Algorithm 2 or Algorithm 1, and obtain  $\Theta^{(t+1)}$ ;
- 4: For given  $\Theta^{(t+1)}$  and  $\mathbf{W}^{(t)}$ , calculate and update  $\mathbf{U}^{(t+1)}$  according to (42);
- 5: For given  $\mathbf{U}^{(t+1)}$ ,  $\mathbf{\Theta}^{(t+1)}$  and  $\mathbf{W}^{(t)}$ , update  $\mathbf{W}^{(t+1)}$  by solving problem (45);
- 6: Calculate  $R\left(\mathbf{W}^{(t+1)}, \mathbf{\Theta}^{(t+1)}\right)$ ;
- 7: Calculate  $\Gamma = \frac{\left|R\left(\mathbf{W}^{(t+1)}, \mathbf{\Theta}^{(t+1)}\right) R\left(\mathbf{W}^{(t)}, \mathbf{\Theta}^{(t)}\right)\right|}{\left|R\left(\mathbf{W}^{(t)}, \mathbf{\Theta}^{(t)}\right)\right|};$
- 8:  $t \leftarrow t + 1$ ;
- 9: end while

# V. NUMERICAL RESULTS

The simulation configurations listed in **TABLE II** are used unless stated otherwise. The following parameter settings were used when executing the beam training schemes for both the hierarchical beam training algorithm for the NN channel model and the second beam training stage for hybrid cascaded channel models. For hierarchical beam training, the sampled range in each direction is set as  $[-1000\lambda_c, 1000\lambda_c]$ . For example, denote the coordinate of the BS antenna midpoint as  $(x_{\rm BS}, y_{\rm BS}, z_{\rm BS})$ , where

TABLE II SIMULATION CONFIGURATIONS

Parameter	Value
Carrier frequency	30GHz
Noise power	-105dBm
Power budget at the BS	30 dBm
Transmitted signal dimension q of NN	2
Transmitted signal dimension q of FF/NF/FN	1
BS's coordinate	(0,0,0)m
User's coordinate	(24,0,0)m
RIS's coordinate	(12, 0, 8)m
Number of BS antennas	8
Number of user antennas	8
Number of RIS elements along $x/y$ -axis	60, 2
Antenna spacing	$\lambda_c/2$

 $z_{\rm BS}$  is fixed. The sampled ranges of the BS in the x- and y-directions are  $[x_{\rm BS}-1000\lambda_c,x_{\rm BS}+1000\lambda_c]$  and  $[y_{\rm BS}-1000\lambda_c,y_{\rm BS}+1000\lambda_c]$ , respectively. The same applies to the sampled ranges of the user. The numbers of sampled points for hierarchical beam training in the x- and y-directions are both set as  $S_x=S_y=2$ . The simulation results are obtained by averaging over 500 channel realizations.

To compare the impact of different channel modeling methods and validate the effectiveness of proposed approach, we conduct numerical simulations on the following schemes:

- NN, Perfect CSI: upper bound, where RIS beamforming is performed with perfect CSI [47];
- NN, Hierarchical: NN channel model, proposed distancebased codebook and hierarchical beam training scheme;
- NN, Uniform ES: NN channel model, the whole sampled range is uniformly divided into several sub-ranges, and the optimal codeword is obtained by exhaustive search<sup>2</sup>;
- NN, Mismatch: NN channel model, angular-domain codebook and beam sweeping;
- NF/FN, Two-stage: hybrid-far-near-field channel model, proposed combined AD codebook and two-stage beam training scheme;
- FF, Angular-domain: FF channel model, angular-domain codebook and beam sweeping.

To determine the number of training layers of the hierarchical beam training scheme, we show the relationship between the achievable rate and the number of training layers in Fig. 4. It can be seen that when  $L_{\rm max} \ge 12$ , the achievable rate no longer increases with  $L_{\rm max}$ . Although the achievable rate only improves slightly from  $L_{\rm max}=2$  to  $L_{\rm max}=12$ , we set the total number of training layers hereafter as  $L_{\text{max}} =$ 12 for better performance. Also, we depict the achievable rate obtained by the ES approach when the number of sampled points is set as 8 and 16 in each direction. The size of the NFC codebook is  $(S_x S_y)^2$ , so it can be extremely large for large  $S_x$ and  $S_y$ . Thus, we only considered two scenarios with small  $S_x$  and  $S_y$  to compare the performance between the proposed hierarchical beam training and ES approaches. Note that we divide the whole sampling range into two sub-ranges in each direction, so there are 4 sampled points in each direction when

 $<sup>^2</sup>$ If the sampling step is too small, the cost of the exhaustive search is unacceptable for the communication system. Therefore, here we divide the entire sampling range into 16 equal intervals in the x and y directions, respectively.

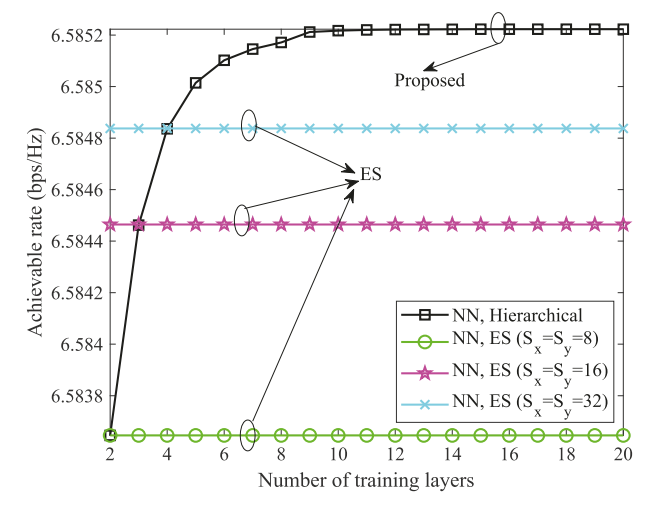


Fig. 4. Achievable rate vs. training layers of hierarchical beam training scheme.

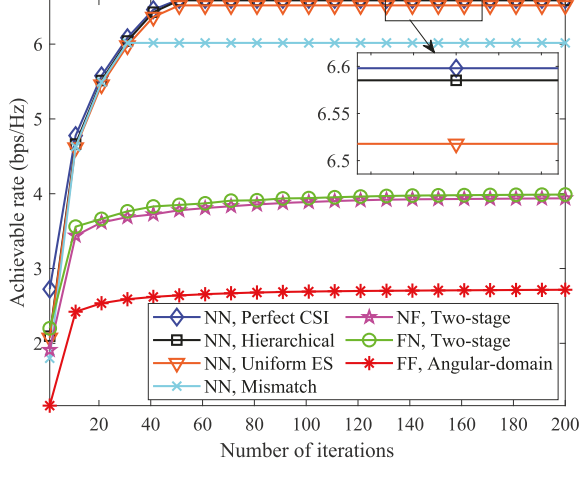


Fig. 6. Convergence performance of the proposed algorithm.

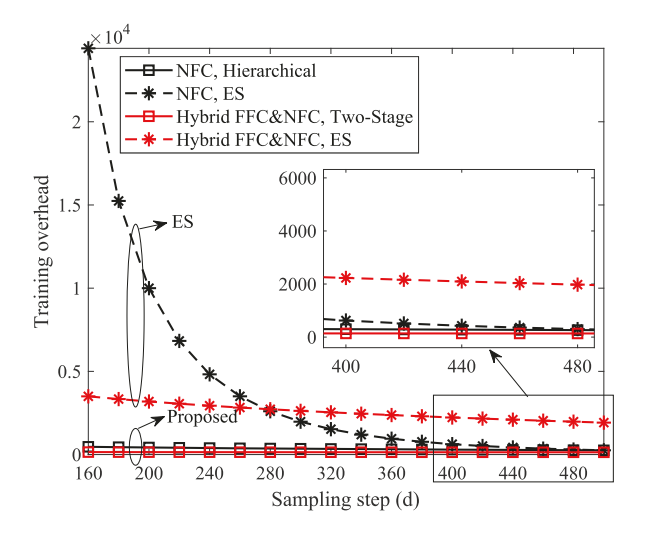


Fig. 5. Beam training overhead vs. sampling step size in multiples of d.

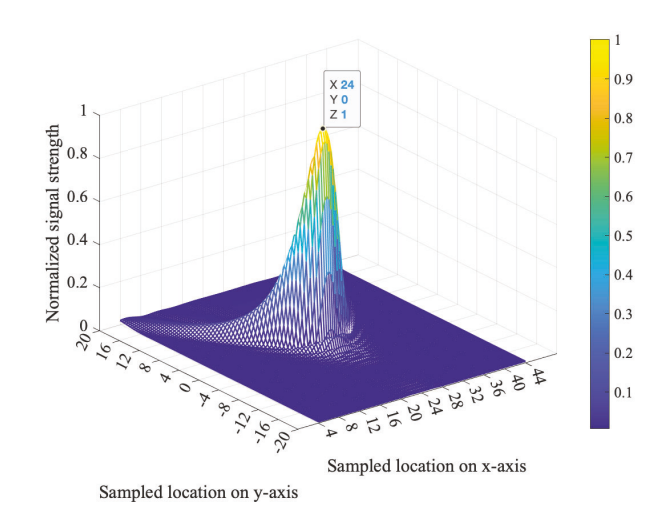


Fig. 7. Normalized received signal strength.

 $S_x=S_y=2$  for hierarchical beam training. Therefore, the proposed hierarchical algorithm achieves the same accuracy as ES with  $S_x=S_y=8$  when the number of training layers is 2, and it is also the same for  $S_x=S_y=16$  when the number of training layers is 3 and for  $S_x=S_y=32$  when the number of training layers is 4, which verifies the effectiveness of our proposed approach which has significantly reduced training costs.

The required beam training overhead of various training algorithms for different sampling step sizes is compared in Fig. 5. For NN channel modeling, the proposed hierarchical near-field beam training approach greatly reduces the training overhead compared to ES beam training, especially when the sampling step size is small. When the step size is 160d, the overhead of the hierarchical beam training approach is only about 2% of that required for ES. When the step size is 500d, these two schemes have the same training overhead, and the required number of training layers for hierarchical beam training is 1. For hybrid FFC & NFC channel models, hierarchical beam training always requires less overhead than ES, regardless of the sampling step size.

The convergence performance of the proposed AO-based algorithm is shown in Fig. 6. Based on the simulation parameters provided earlier, we can calculate that both the BS-RIS and RIS-user links are within the near-field region. Since the NN channel model with hierarchical beam training is more accurate since it considers both angular and distance information of the cascaded links, it will provide a higher achievable rate. Furthermore, it can be seen that the obtained rate by the proposed hierarchical beam training is very close to that of the RIS beamforming with perfect CSI, while the computational complexity significantly reduced. Although the uniform ES scheme is also very close to the upper bound, its overhead is much higher than the proposed scheme. Even though the NN channel model is adopted, the performance obtained with mismatched beam training is poor, because distance information is not considered. The FF channel model has the worst performance due to the accumulative channel estimation error of links on both sides of the RIS.

For the NN channel model, the normalized received signal strength is depicted in Fig. 7. We can see that the maximum

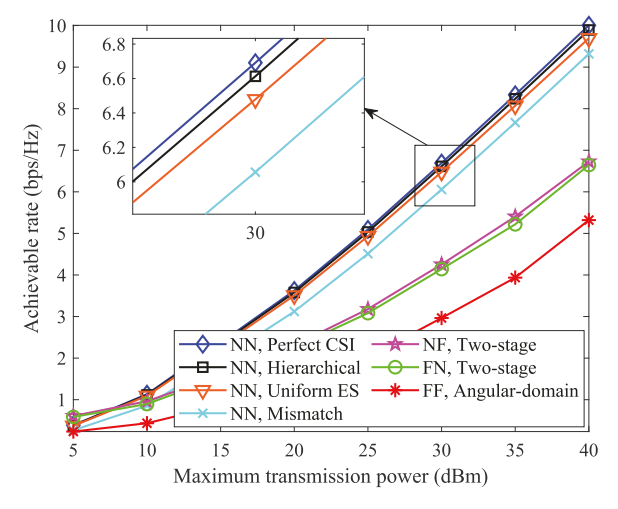


Fig. 8. Achievable rate vs. maximum transmission power at the BS.

received power appears at coordinate (24, 0), which is exactly where the user is located. Since the user's antennas are distributed parallel to the x-axis, the received signal strength is also dispersed along the x-axis. Moreover, the RIS reflecting elements are more distributed along the x-axis direction, which will also lead to such a distribution of reflected signals. Unlike FFC, NFC can achieve beam focusing, concentrating the energy of the beam at a specific location.

In Fig. 8, we show the relationship between the achievable rate and the power budget at the BS. As expected, regardless of the channel model or beam training approach, the achievable rate increases with the BS power budget. In addition, for low BS power, NN with hierarchical beam training cannot fully leverage its advantages for accurate channel estimation, thus having a lower achievable rate than NF and FN. As the power increases, the achievable rate of NN increases the fastest, and its performance advantages become increasingly pronounced compared to the other models. The rates achieved with the NF and FN channel models are nearly the same for all power levels, since the BS-RIS and RIS-user distances remain the same, the number of antennas equipped by BS and user is the same, and the same beam training methods are used for both. Furthermore, the performance of the proposed hierarchical beam training is always approximately equal to that under perfect CSI and superior to other comparison schemes, which verifies the effectiveness of the proposed scheme.

Fig. 9 shows the achievable rate for different numbers of RIS reflecting elements M. The achievable rate for all channel model and beam training approaches increases with M, due to the higher passive array gains that can be obtained from larger RIS. The NN channel model achieves the fastest increase in rate as M increases since the near-field effect is greater for larger RISs, the NN model describes the channel more accurately, and the hierarchical beam training approach realizes a more effective beam focusing. Furthermore, the achievable rate obtained using the NN channel model with angular-domain beam training will be superior to that of the FF model due to the more accurate channel information, even if the utilized beam training approach is not specifically designed for the NN model.

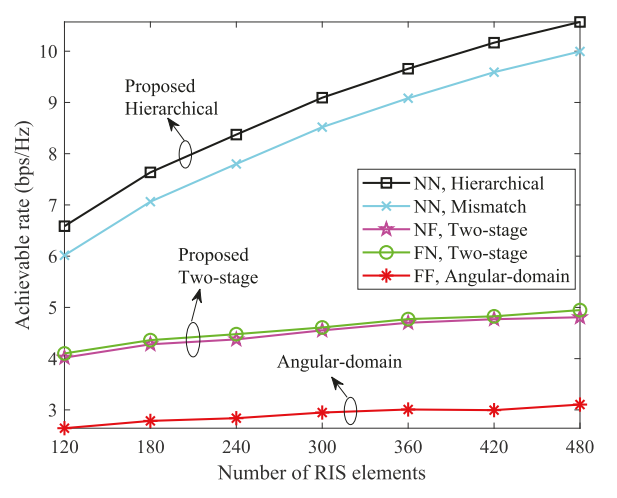


Fig. 9. Achievable rate vs. number of RIS elements.

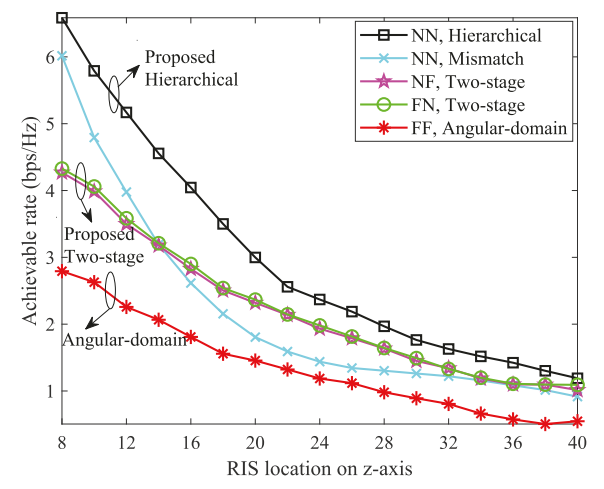


Fig. 10. Achievable rate vs. RIS location on z-axis.

Fig. 10 shows the achievable rate as the RIS is located at different points in the z-direction. Note that the z coordinates of both the BS and the user are 0. For smaller z values, the closer the RIS is to the BS and user, the more obvious the near-field effect. Therefore, the performance gain of adopting NN channel models and hierarchical beam training is more significant with smaller z, and the results are consistent with that in Fig. 6 when z=8. Moreover, as the distance between the RIS and BS and the user gradually increases, the performance gap due to different channel models and beam training methods gradually decreases. It can be predicted that when z is large enough, these curves will eventually coincide, which also verifies that the near-field channel can be approximated as the far-field channel.

The achievable rate obtained for different RIS locations along the x-direction is depicted in Fig. 11. It is not difficult to see that the NN channel model with hierarchical beam training always has the highest rate, regardless of the RIS location. In addition, for the NN channel model, a peak appears on both the BS and user side, which is consistent with the conclusions for FFC. For the NF channel model, the maximum achievable rate is obtained with the RIS near the BS, due to the more obvious near-field effect of the BS-RIS link. As the RIS moves away from the BS, the achievable rate decreases, although this

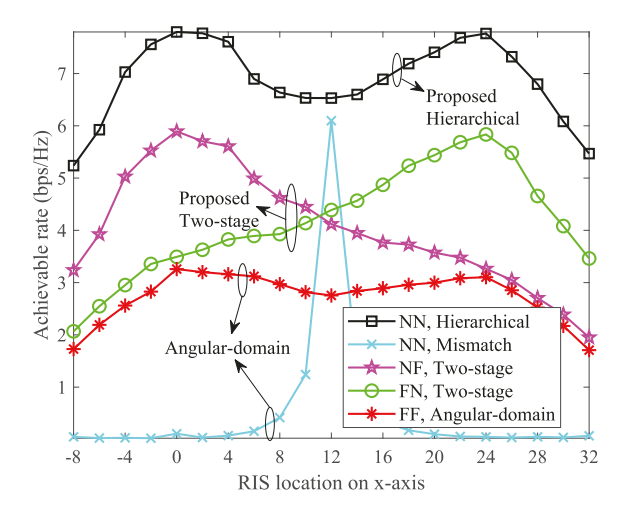


Fig. 11. Achievable rate vs. RIS location on x-axis.

degradation in rate slows near the user's location. For the FN channel model, in contrast to NF, the peak appears around the user. When adopting the NN channel model and angular beam training, a peak occurs only when the RIS is deployed at an equal distance between the BS and the user, which means that angular beam training for the NN model is only useful in restricted scenarios.

#### VI. CONCLUSION

In this article, we considered four different channel models for a RIS-assisted downlink MIMO system. According to the angular or distance information embedded in the received signals under these specific channel models, we designed different codebooks to match the beam steering vectors for the RIS. Based on the predesigned codebooks, we proposed two beam training approaches, which were further used for RIS coefficient optimization. More specifically, for the NN channel model, we designed a distance-based codebook and proposed a hierarchical beam training algorithm to realize beam alignment while reducing the training overhead; for the NF and FN channel models, we designed a combined angular-distance codebook and proposed a two-stage beam training approach to separately realize beam alignment in the angular- and distance domains. To maximize the achievable rate, we proposed an AO-based algorithm to carry out the multi-resource optimization in an iterative manner. Numerical results show that the proposed beam training approaches can obtain achievable rate performance similar to the ES method, while significantly reducing the training overhead. Our results demonstrate that the use of distance in addition to angular information can effectively improve the system performance with near-field channels.

#### REFERENCES

- I. F. Akyildiz, C. Han, and S. Nie, "Combating the distance problem in the millimeter wave and terahertz frequency bands," *IEEE Commun. Mag.*, vol. 56, no. 6, pp. 102–108, Jun. 2018.
- [2] C. Castro, R. Elschner, T. Merkle, C. Schubert, and R. Freund, "Experimental demonstrations of high-capacity THz-wireless transmission systems for beyond 5G," *IEEE Commun. Mag.*, vol. 58, no. 11, pp. 41–47, Nov. 2020.

- [3] K. M. S. Huq, J. Rodriguez, and I. E. Otung, "3D network modeling for THz-enabled ultra-fast dense networks: A 6G perspective," *IEEE Commun. Standards Mag.*, vol. 5, no. 2, pp. 84–90, Jun. 2021.
- [4] C. Lin, G. Y. Li, and L. Wang, "Subarray-based coordinated beamforming training for mmWave and sub-THz communications," *IEEE J. Sel. Areas Commun.*, vol. 35, no. 9, pp. 2115–2126, Jun. 2017.
- [5] C. Pradhan, A. Li, L. Song, B. Vucetic, and Y. Li, "Hybrid precoding design for reconfigurable intelligent surface aided mmWave communication systems," *IEEE Wireless Commun. Lett.*, vol. 9, no. 7, pp. 1041–1045, Jul. 2020.
- [6] C. Huang et al., "Multi-hop RIS-empowered terahertz communications: A DRL-based hybrid beamforming design," *IEEE J. Sel. Areas Commun.*, vol. 39, no. 6, pp. 1663–1677, Jun. 2021.
- [7] M. Di Renzo et al., "Smart radio environments empowered by reconfigurable intelligent surfaces: How it works, state of research, and the road ahead," *IEEE J. Sel. Areas Commun.*, vol. 38, no. 11, pp. 2450–2525, Nov. 2020.
- [8] H. Lu and Y. Zeng, "Communicating with extremely large-scale array/surface: Unified modeling and performance analysis," *IEEE Trans. Wireless Commun.*, vol. 21, no. 6, pp. 4039–4053, Jun. 2022.
- [9] H. Zhang et al., "Beam focusing for near-field multiuser MIMO communications," *IEEE Trans. Wireless Commun.*, vol. 21, no. 9, pp. 7476–7490, Sep. 2022.
- [10] Y. Liu, Z. Wang, J. Xu, C. Ouyang, X. Mu, and R. Schober, "Near-field communications: A tutorial review," *IEEE Open J. Commun. Soc.*, vol. 4, pp. 1999–2049, 2023.
- [11] Y. Jiang, F. Gao, M. Jian, S. Zhang, and W. Zhang, "Reconfigurable intelligent surface for near field communications: Beamforming and sensing," *IEEE Trans. Wireless Commun.*, vol. 22, no. 5, pp. 3447–3459, May 2023.
- [12] P. Mei et al., "On the study of reconfigurable intelligent surfaces in the near-field region," *IEEE Trans. Antennas Propag.*, vol. 70, no. 10, pp. 8718–8728, Oct. 2022.
- [13] X. Zhang and H. Zhang, "Hybrid reconfigurable intelligent surfacesassisted near-field localization," *IEEE Commun. Lett.*, vol. 27, no. 1, pp. 135–139, Jan. 2023.
- [14] Q. Yang, R. He, and B. Ai, "SNR analysis for RIS-aided communication system in near- and far-fields," in *Proc. 14th Int. Conf. Wireless Commun. Signal Process. (WCSP)*, Nov. 2022, pp. 1001–1006.
- [15] S. Yang, W. Lyu, Z. Hu, Z. Zhang, and C. Yuen, "Channel estimation for near-field XL-RIS-aided mmWave hybrid beamforming architectures," *IEEE Trans. Veh. Technol.*, vol. 72, no. 8, pp. 11029–11034, Aug. 2023.
- [16] X. Yu, W. Shen, R. Zhang, C. Xing, and T. Q. S. Quek, "Channel estimation for XL-RIS-aided millimeter-wave systems," *IEEE Trans. Commun.*, vol. 71, no. 9, pp. 5519–5533, Sep. 2023.
- [17] Y. Pan, C. Pan, S. Jin, and J. Wang, "RIS-aided near-field localization and channel estimation for the terahertz system," *IEEE J. Sel. Topics Signal Process.*, vol. 17, no. 4, pp. 878–892, Jul. 2023.
- [18] J. Zhang, Y. Huang, Q. Shi, J. Wang, and L. Yang, "Codebook design for beam alignment in millimeter wave communication systems," *IEEE Trans. Commun.*, vol. 65, no. 11, pp. 4980–4995, Nov. 2017.
- [19] C. Qi, K. Chen, O. Dobre, and G. Y. Li, "Hierarchical codebook-based multiuser beam training for millimeter wave massive MIMO," *IEEE Trans. Wireless Commun.*, vol. 19, no. 12, pp. 8142–8152, Dec. 2020.
- [20] Y. Zhang, X. Wu, and C. You, "Fast near-field beam training for extremely large-scale array," *IEEE Wireless Commun. Lett.*, vol. 11, no. 12, pp. 2625–2629, Dec. 2022.
- [21] P. Wang, J. Fang, W. Zhang, Z. Chen, H. Li, and W. Zhang, "Beam training and alignment for RIS-assisted millimeter-wave systems: State of the art and beyond," *IEEE Wireless Commun.*, vol. 29, no. 6, pp. 64–71, Dec. 2022.
- [22] J. Wang, W. Tang, S. Jin, C.-K. Wen, X. Li, and X. Hou, "Hierarchical codebook-based beam training for RIS-assisted mmWave communication systems," *IEEE Trans. Commun.*, vol. 71, no. 6, pp. 3650–3662, Jun. 2023.
- [23] W. Liu, C. Pan, H. Ren, F. Shu, S. Jin, and J. Wang, "Low-overhead beam training scheme for extremely large-scale RIS in near field," *IEEE Trans. Commun.*, vol. 71, no. 8, pp. 4924–4940, Aug. 2023.
- [24] X. Wei and L. Dai, "Channel estimation for extremely large-scale massive MIMO: Far-field, near-field, or hybrid-field?" *IEEE Commun. Lett.*, vol. 26, no. 1, pp. 177–181, Jan. 2022.

- [25] Z. Hu, C. Chen, Y. Jin, L. Zhou, and Q. Wei, "Hybrid-field channel estimation for extremely large-scale massive MIMO system," *IEEE Commun. Lett.*, vol. 27, no. 1, pp. 303–307, Jan. 2023.
- [26] M. Cui and L. Dai, "Channel estimation for extremely large-scale MIMO: Far-field or near-field?" *IEEE Trans. Commun.*, vol. 70, no. 4, pp. 2663–2677, Apr. 2022.
- [27] Z. Yuan, J. Zhang, Y. Ji, G. F. Pedersen, and W. Fan, "Spatial non-stationary near-field channel modeling and validation for massive MIMO systems," *IEEE Trans. Antennas Propag.*, vol. 71, no. 1, pp. 921–933, Jan. 2023.
- [28] S.-G. Yoon and S. J. Lee, "Improved hierarchical codebook-based channel estimation for mmWave massive MIMO systems," IEEE Wireless Commun. Lett., vol. 11, no. 10, pp. 2095–2099, Oct. 2022.
- [29] C. Wu, C. You, Y. Liu, L. Chen, and S. Shi, "Two-stage hierarchical beam training for near-field communications," 2023, arXiv:2302.12511.
- [30] X. Shi, J. Wang, Z. Sun, and J. Song, "Spatial-chirp codebook-based hierarchical beam training for extremely large-scale massive MIMO," *IEEE Trans. Wireless Commun.*, vol. 23, no. 4, pp. 2824–2838, Apr. 2024.
- [31] Y. Zhang, B. Di, H. Zhang, M. Dong, L. Yang, and L. Song, "Dual codebook design for intelligent omni-surface aided communications," *IEEE Trans. Wireless Commun.*, vol. 21, no. 11, pp. 9232–9245, Nov. 2022.
- [32] C. You, B. Zheng, and R. Zhang, "Fast beam training for IRS-assisted multiuser communications," *IEEE Wireless Commun. Lett.*, vol. 9, no. 11, pp. 1845–1849, Nov. 2020.
- [33] D. Shen, L. Dai, X. Su, and S. Suo, "Multi-beam design for near-field extremely large-scale RIS-aided wireless communications," *IEEE Trans. Green Commun. Netw.*, vol. 7, no. 3, pp. 1542–1553, Sep. 2023.
- [34] X. Wei, L. Dai, Y. Zhao, G. Yu, and X. Duan, "Codebook design and beam training for extremely large-scale RIS: Far-field or near-field?" *China Commun.*, vol. 19, no. 6, pp. 193–204, Jun. 2022.
- [35] D. De Donno, J. Palacios, and J. Widmer, "Millimeter-wave beam training acceleration through low-complexity hybrid transceivers," *IEEE Trans. Wireless Commun.*, vol. 16, no. 6, pp. 3646–3660, Jun. 2017.
- [36] O. El. Ayach, S. Rajagopal, S. Abu-Surra, Z. Pi, and R. W. Heath, "Spatially sparse precoding in millimeter wave MIMO systems," *IEEE Trans. Wireless Commun.*, vol. 13, no. 3, pp. 1499–1513, Jan. 2014.
- [37] M. R. Akdeniz et al., "Millimeter wave channel modeling and cellular capacity evaluation," *IEEE J. Sel. Areas Commun.*, vol. 32, no. 6, pp. 1164–1179, Jun. 2014.
- [38] X. Gao, L. Dai, S. Han, and R. W. Heath Jr., "Energy-efficient hybrid analog and digital precoding for mmWave MIMO systems with large antenna arrays," *IEEE J. Sel. Areas Commun.*, vol. 34, no. 4, pp. 998–1009, Apr. 2016.
- [39] C. Ouyang, Y. Liu, X. Zhang, and L. Hanzo, "Near-field communications: A degree-of-freedom perspective," 2023, arXiv:2308.00362.
- [40] M. Cui and L. Dai, "Near-field wideband beamforming for extremely large antenna arrays," 2021, arXiv:2109.10054.
- [41] Y. Liu, J. Xu, Z. Wang, X. Mu, and L. Hanzo, "Near-field communications: What will be different?" 2023, arXiv:2303.04003.
- [42] F. Sohrabi and W. Yu, "Hybrid digital and analog beamforming design for large-scale antenna arrays," *IEEE J. Sel. Topics Signal Process.*, vol. 10, no. 3, pp. 501–513, Apr. 2016.
- [43] X. Mu, J. Xu, Y. Liu, and L. Hanzo, "Reconfigurable intelligent surface-aided near-field communications for 6G: Opportunities and challenges," *IEEE Veh. Technol. Mag.*, vol. 19, no. 1, pp. 65–74, Mar. 2024.
- [44] Q. Shi, M. Razaviyayn, Z.-Q. Luo, and C. He, "An iteratively weighted MMSE approach to distributed sum-utility maximization for a MIMO interfering broadcast channel," *IEEE Trans. Signal Process.*, vol. 59, no. 9, pp. 4331–4340, Sep. 2011.
- [45] B. Zheng, C. You, and R. Zhang, "Double-IRS assisted multi-user MIMO: Cooperative passive beamforming design," *IEEE Trans. Wireless Commun.*, vol. 20, no. 7, pp. 4513–4526, Jul. 2021.
- [46] M. S. Lobo, L. Vandenberghe, S. Boyd, and H. Lebret, "Applications of second-order cone programming," *Linear Algebra Appl.*, vol. 284, no. 1, pp. 193–228, 1998. [Online]. Available: https://www.sciencedirect.com/science/article/pii/S0024379598100320

[47] J. He, H. Wymeersch, and M. Juntti, "Channel estimation for RIS-aided mmWave MIMO systems via atomic norm minimization," *IEEE Trans. Wireless Commun.*, vol. 20, no. 9, pp. 5786–5797, Sep. 2021.



Suyu Lv (Graduate Student Member, IEEE) received the bachelor's degree in communication engineering from Beijing University of Posts and Telecommunications (BUPT), Beijing, China, in 2018, where she is currently pursuing the Ph.D. degree in information and communication engineering with the State Key Laboratory of Networking and Switching Technology. From November 2022 to September 2023, she was a Visiting Student with the School of Electronic Engineering and Computer Science, Queen Mary University of

London, London, U.K. Her main research interests include finite blocklength transmission, reconfigurable intelligent surface, and non-orthogonal multiple access



Yuanwei Liu (Fellow, IEEE) received the Ph.D. degree in electrical engineering from the Queen Mary University of London, U.K., in 2016. He was with the Department of Informatics, King's College London, from 2016 to 2017, where he was a Post-Doctoral Research Fellow. He has been a Senior Lecturer (Associate Professor) with the School of Electronic Engineering and Computer Science, Queen Mary University of London, since August 2021, where he was a Lecturer (Assistant Professor) from 2017 to 2021. His research interests include

non-orthogonal multiple access, reconfigurable intelligent surface, near field communications, integrated sensing and communications, and machine learning.

He is a fellow of AAIA, a Web of Science Highly Cited Researcher, an IEEE Communication Society Distinguished Lecturer, an IEEE Vehicular Technology Society Distinguished Lecturer, the Rapporteur of ETSI Industry Specification Group on Reconfigurable Intelligent Surfaces on work item of "Multi-Functional Reconfigurable Intelligent Surfaces (RIS): Modelling, Optimisation, and Operation," and the U.K. Representative for the URSI Commission C on "Radio Communication Systems and Signal Processing." He was listed as one of 35 Innovators Under 35 China in 2022 by MIT Technology Review. He received IEEE ComSoc Outstanding Young Researcher Award for EMEA in 2020. He received the 2020 IEEE Signal Processing and Computing for Communications (SPCC) Technical Committee Early Achievement Award and IEEE Communication Theory Technical Committee (CTTC) 2021 Early Achievement Award. He received IEEE ComSoc Outstanding Nominee for Best Young Professionals Award in 2021. He was a co-recipient of the Best Student Paper Award in IEEE VTC2022-Fall, the Best Paper Award in ISWCS 2022, the 2022 IEEE SPCC-TC Best Paper Award, the 2023 IEEE ICCT Best Paper Award, and the 2023 IEEE ISAP Best Emerging Technologies Paper Award. He serves as the Co-Editor-in-Chief for IEEE ComSoc TC Newsletter; an Area Editor for IEEE COMMUNICATIONS LETTERS; and an Editor for IEEE COMMUNICATIONS SURVEYS & TUTORIALS, IEEE TRANSACTIONS ON WIRELESS COMMUNICATIONS, IEEE TRANSACTIONS ON VEHICULAR TECHNOLOGY, IEEE TRANSACTIONS ON NETWORK SCIENCE AND ENGINEERING, and IEEE TRANSACTIONS ON COMMUNICATIONS (2018-2023). He serves as the (leading) Guest Editor for PROCEEDINGS OF THE IEEE on Next Generation Multiple Access, IEEE JOURNAL ON SELECTED AREAS IN COMMUNICATIONS on Next Generation Multiple Access, IEEE JOURNAL OF SELECTED TOPICS IN SIGNAL PROCESSING on Intelligent Signal Processing and Learning for Next Generation Multiple Access, and IEEE Network on Next Generation Multiple Access for 6G. He serves as the Publicity Co-Chair for IEEE VTC 2019-Fall, the Panel Co-Chair for IEEE WCNC 2024, and the Symposium Co-Chair for several flagship conferences, such as IEEE GLOBECOM, ICC, and VTC. He serves as the Academic Chair for the Next Generation Multiple Access Emerging Technology Initiative and the Vice Chair for SPCC and Technical Committee on Cognitive Networks (TCCN). For more information visit the link (http://www.eecs.qmul.ac.uk/ yuanwei).



**Xiaodong Xu** (Senior Member, IEEE) received the B.S. degree in information and communication engineering and the master's degree in communication and information system from Shandong University in 2001 and 2004, respectively, and the Ph.D. degree in circuit and system from Beijing University of Posts and Telecommunications (BUPT) in 2007. He is currently a Professor with BUPT, a Research Fellow of the Department of Broadband Communication, Peng Cheng Laboratory, and a member of IMT-2030 (6G) Experts Panel. He has coauthored

nine books/chapters and more than 120 journals and conference papers. He is also an inventor or the co-inventor of 51 granted patents. His research interests cover semantic communications, intelligent communication systems, moving networks, mobile edge computing, and caching.



Arumugam Nallanathan (Fellow, IEEE) has been a Professor in wireless communications and the Head of the Communication Systems Research (CSR) Group, School of Electronic Engineering and Computer Science, Queen Mary University of London, since September 2017. He was with the Department of Informatics, King's College London, from December 2007 to August 2017, where he was a Professor in wireless communications from April 2013 to August 2017 and a Visiting Professor from September 2017 to August 2020. He was

an Assistant Professor with the Department of Electrical and Computer Engineering, National University of Singapore, from August 2000 to December 2007. He has published nearly 700 technical papers in scientific journals and international conferences. His research interests include artificial intelligence for wireless systems, beyond 5G wireless networks, and the Internet of Things (IoT).

He was a co-recipient of the Best Paper Awards presented at the IEEE International Conference on Communications 2016 (ICC'2016), IEEE Global Communications Conference 2017 (GLOBECOM'2017), and IEEE Vehicular

Technology Conference 2018 (VTC'2018). He was a co-recipient of IEEE Communications Society Leonard G. Abraham Prize in 2022. He is an IEEE Distinguished Lecturer. He has been selected as a Web of Science Highly Cited Researcher in 2016, 2022, and 2023. He received the IEEE Communications Society SPCE Outstanding Service Award in 2012 and IEEE Communications Society RCC Outstanding Service Award in 2014. He served as the Chair for the Signal Processing and Communication Electronics Technical Committee of IEEE Communications Society and Technical Program Chair and a member of technical program committees in numerous IEEE conferences. He was a Senior Editor of IEEE WIRELESS COMMUNICATIONS, LETTERS and an Editor of IEEE TRANSACTIONS ON WIRELESS COMMUNICATIONS, IEEE TRANSACTIONS ON VEHICULAR TECHNOLOGY, and IEEE SIGNAL PROCESSING LETTERS.



A. Lee Swindlehurst (Fellow, IEEE) received the B.S. and M.S. degrees in electrical engineering from Brigham Young University (BYU) in 1985 and 1986, respectively, and the Ph.D. degree in electrical engineering from Stanford University in 1991. He was with the Department of Electrical and Computer Engineering, BYU, from 1990 to 2007 and from 1996 to 1997, he held a joint appointment as a Visiting Scholar with Uppsala University and the Royal Institute of Technology, Sweden. From 2006 to 2007, he was on leave

working as the Vice President of Research with ArrayComm LLC, San Jose, CA, USA. Since 2007, he has been with the Electrical Engineering and Computer Science (EECS) Department, University of California at Irvine, where he is currently a Distinguished Professor and holds the Nicolaos G. and Sue Curtis Alexopoulos Presidential Chair. From 2014 to 2017, he was also a Hans Fischer Senior Fellow of the Institute for Advanced Studies, Technical University of Munich. In 2016, he was elected as a Foreign Member of the Royal Swedish Academy of Engineering Sciences (IVA). His research focuses on array signal processing for radar, wireless communications, and biomedical applications. He was the inaugural Editor-in-Chief of the IEEE JOURNAL OF SELECTED TOPICS IN SIGNAL PROCESSING. He received the 2000 IEEE W. R. G. Baker Prize Paper Award, the 2006 IEEE Communications Society Stephen O. Rice Prize in the Field of Communication Theory, the 2006, 2010, and 2021 IEEE Signal Processing Society's Best Paper Awards, the 2017 IEEE Signal Processing Society Donald G. Fink Overview Paper Award, a Best Paper Award at the 2020 IEEE International Conference on Communications, and the 2022 Claude Shannon-Harry Nyquist Technical Achievement Award from the IEEE Signal Processing Society.